UNIVERSITY OF OKLAHOMA

GRADUATE COLLEGE

ROCK CHARACTERIZATION AND STRATIGRAPHY OF THE MISSISSIPPIAN STRATA, MERAMEC / SYCAMORE. MERGE PLAY, CENTRAL OKLAHOMA

A THESIS

SUBMITTED TO THE GRADUATE FACULTY

in partial fulfillment of the requirements for the

Degree of

MASTER OF SCIENCE

By

DAVID ENRIQUE DUARTE CORONADO

Norman, Oklahoma

2018

ROCK CHARACTERIZATION AND STRATIGRAPHY OF THE MISSISSIPPIAN STRATA, MERAMEC / SYCAMORE. MERGE PLAY, CENTRAL OKLAHOMA

A THESIS APPROVED FOR THE

CONOCOPHILLIPS SCHOOL OF GEOLOGY AND GEOPHYSICS

BY

Dr. Roger Slatt, Chair

Dr. Matthew Pranter

Dr. Douglas Elmore

To my grandma Eloisa, the best example that anyone could have.

ACKNOWLEDGMENTS

First, I want to express my most sincere gratitude to Dr. Roger Slatt for believing in me and giving me the opportunity to be part of the Institute for Reservoir Characterization (IRC). His hard work, passion for the geology, commitment with the field, and work ethics will be my inspiration throughout my career. Thank you for supporting my research, the advancement of my career, and for being a model for all the students.

My gratitude is also extended to my thesis committee members, Dr. Douglas Elmore, and Dr. Matthew Pranter, for their valuable comments and constructive criticism which led to the improvement of my research. I also want to thank the staff of the ConocoPhillips School of Geology and Geophysics at the University of Oklahoma, especially Rebecca Fay for her kind willingness to support me and guide me at navigating my graduate degree.

Thanks to current and previous members from the Institute of Reservoir Characterization for their professional and personal support. Their friendship is one of the most important outcomes from my master's degree. Thanks to Andreina, Benmadi, Brian, David P., Delcio, Javier, Jing, Muizz, Nya, Zainab. Special thanks go to Carlos M., Daniela, Emilio, Henry, and Richard for their precious contributions and discussions through the development of this manuscript. Thanks to Rafael and Gabriel who accompanied me during this journey and contributed with significant and fresh perspectives from their study areas.

Thanks to all the people and companies that supported my research and education through the STACK–MERGE–SCOOP consortium (formerly Woodford consortium), especially to Kevin

Morgan whom proposed this project and provided some data through Jones Energy. I also want to thank the staff of the Oklahoma Petroleum Information Center (OPIC) for their collaboration laying out and sampling the cores that compose this thesis. My sincere gratitude goes to Vyetta and Jeff for their kindness and willingness to collaborate with everything I needed to successfully complete this research.

Finally, the greatest of the gratitude goes for my family, my mom, dad, sister, and grandma. They are my inspiration and motivation to continuously set and achieve new personal and professional goals. Thanks to my beloved Alejandra Hernández for being my partner in crime throughout this adventure. Her love, intelligence, and support encourage me to continue pursuing my dreams even in the hardest moments that life might bring on.

“The journey of a thousand miles begins with one step” -Lao Tzu

TABLE OF CONTENTS

List of figures ix

List of tables xiii

ABSTRACT xiv

1. INTRODUCTION 1

2. GEOLOGICAL SETTINGS IN THE ANADARKO BASIN 4

2.1 Structural framework 4

2.2 Stratigraphy 5

3. METHODS AND MATERIALS 8

3.1. Petrographic analysis 10

3.2. Isotopic analysis ($\delta^{13}C‰$ and $\delta^{18}O‰$) 11

3.3 Elemental composition from X-ray fluorescence spectroscopy 12

3.4 Determination of chemofacies based on cluster analysis 14

3.5 Sequence stratigraphy 16

3.6 Organic geochemistry 17

3.7 Porosity/Permeability 19

3.8 Rock hardness (micro-Rebound hammer) 19

3.9 Mapping 19

4. RESULTS 21

4.1 Petrology 21

4.1.1. Detrital composition 24

4.1.2. Diagenetic minerals and cements 26

4.2 Carbon and oxygen isotopes ($\delta^{13}C‰$ and $\delta 18O‰$) 28

4.3 Elemental composition variability 30

4.4 Optimal number of clusters 33

4.5 Chemofacies: zones with similar elemental composition 35

4.6 Variation in elemental composition during Mississippian time 39

4.7 Sequence stratigraphy 39

4.8 Reservoir quality 42

4.8.1 Porosity and permeability data 44

4.8.2 Hardness 47

4.8.3 Organic geochemistry 48
4.8.4 Map 51
5. DISCUSSION 53
5.1. Stratigraphic description 53
5.2. Diagenesis and origin of the calcite cement 54
5.3. Time framework 60
5.4. Sequence stratigraphy 63
5.5. Reservoir quality 66
CONCLUSIONS 69
REFERENCES 71

LIST OF FIGURES

Figure 1: early Mississippian pelotopographic map and location map. It shows the location of the area of study in central Oklahoma. Geological provinces in Oklahoma (bottom right). Skaggs and Payne (red stars) cores located in Grady and Canadian counties (Anadarko basin), respectively (bottom left). More than 800 wells, the green dots are oil wells and red dots are gas wells in the area of study from HIS databased (bottom left). Modified from Blakey, 2013; Gutschick and Sandberg, 1983 5

Figure 2 Mississippian stratigraphy from the Anadarko basin , based on different studies (Bennison, 1956; Braun, 1961; Culp, 1961; Curtis and Champlin, 1959; Peace, 1994). 6

Figure 3: Skaggs and Payne cores profile with 2-inch vertical spacing; core gamma-ray, lithofacies, elemental composition and chemofacies. Lithofacies; Massive calcite-cemented siltstone (MCcSt), Calcareous siltstone (CSt), Bioturbated siltstone (BSt), Laminated siltstone (LSt), Bioturbated mudstone (BMdst), Laminated mudstone (LMdst), Interbedded siltstone (ISt), calcite cement (Ccmt), strata around the unconformity (Post), glauconitic sandstone (GS), and Woodford shale (Wdfd).Chemofacies are related with the elemental composition in the following manner: blue chemofacies with high Calcium and Strontium; light blue with high Mg; red with high Si/Al and Zr; Green and Yellow chemofacies are distributed in low calcite-cemented lithofacies with similar elemental composition but differ in that yellow chemofacies has slightly more Ti, K, and Al, and the green chemofacies has more Molybdenum. 10

Figure 4: thin section photos from the facies found in Mississippian strata. A) massive calcite cemented siltstone (MCcSt) B) calcite cement (Ccmt) C) bioturbated siltstone (BSt) D) laminated siltstone (LSt) E) calcareous siltstone (CSt) F) Bioturbated mudstone (BMdst) G) laminated mudstone (LMdst) H) Interbedded siltstone (ISt)..... 22

Figure 5: contact between the Woodford shale and Mississippian strata. A) core (Skaggs) photo of the contact. B) thin section photo of the Woodford shale below the unconformity. C) thin section photo of the glauconitic sandstone (GS) in the Mississippian rocks overlying the Woodford shale.. 23

Figure 6: Mississippian/Pennsylvanian contact. A) core (Payne) photo of the contact with the location of the thin sections to the right. B) thin section photo of the Silty micrite at 8901 ft. C) Sparitic siltstone at 8898 ft. D) quartz-rich fine sandstone at 8895 ft. For future reference in the isotopes analysis, samples B, C and D are named “Post”..... 24

Figure 7: Petrographic photos of the Massive calcite-cemented siltstones (MCcSt). A) sample Payne 015 at depth 8942.0, parallel Nicols B) crossed Nicols C) sample Payne 003 at depth 8954.0, parallel Nicolls D) crossed Nicolls. 25

Figure 8: element maps for a sample in Payne core at 8954 ft. A) elemental map of Mg, Fe, Ca, K, Al, Na, and Ti B) calcium map. C) magnesium map D) iron map. Rhombic dolomite crystal enriched in iron at the borders. 27

Figure 9: SEM photomicrographs. A) structural organic matter, Skaggs 9737.5 ft. B) detail of Figure 9.A. oil drop. C) pyrite framboids, Payne 8958.5 ft. D) detrital zircon, Skaggs 9741.0 ft. E) blocky calcite cement, Skaggs 9731.0 ft. F) dolomite cement surrounding calcareous grains, Skaggs 9731.0 ft..... 28

Figure 10: δ^{13} C vs δ^{18} O for Mississippian rocks in the Skaggs and Payne cores. It shows three main clusters: cluster I in blue (MCcSt), cluster II (lithofacies with low calcite content) in yellow and cluster III in green (samples were taken around the unconformity, named "Post"). 29

Figure 11: carbonate and clay proxies cross plots A) Relation between carbonate source proxies (Ca vs Sr). Two differentiated trends are controlled by lithofacies. While the linear direct relation is given mainly by low calcite facies, in the MCcSt lithofacies the Ca content increase with constant Sr composition. B) Relation between clay proxies (Al vs K). The cross plot differentiates two trends not controlled by lithofacies. The trend with higher slope is restricted to the lowermost section in the Payne core. 32

Figure 12: Silhouette and Elbow methods to select the optimal number of clusters. Silhouette (upper) and Elbow (lower) methods were used to define the number of clusters used as an input in the K-means clustering algorithm. In the Silhouette method, a high value indicates good match and a low value indicates a poor match. The Elbow method measured the distance of an object within a cluster. After 4 or 6 number of clusters, the data does not change significantly. 34

Figure 13: PC1 vs PC2 cross plot using the clusters from K-means as a grouping variable. The original variables (orange arrows) were plotted to illustrate the key elements on each chemofacies..... 36

Figure 14:distribution of the lithofacies within the chemofacies. Dark blue chemofacies is related with high Calcium content; light blue with high Magnesium; red with high Si/Al and Zirconium; yellow is related with high Potassium, Titanium, and Aluminum; and green with high Mo. 38

Figure 15: photo and scheme of the Mississippian strata in the Payne core. Photo of the core (left) and the scheme of the relationship between lithofacies (right). Massive calcite-cemented

siltstone (MCcSt) is bounded at the base by a sharp erosional contact (A) and at the top by a transitional contact (B). 40

Figure 16: Gamma-ray parasequence or third-order sequences superimposed by fourth-order sequences. Black rectangles to the left represent the cored section in Payne (left) and Skaggs(right) wells. The gamma-ray parasequences are interpreted from the well-log rather than the core gamma scan. 42

Figure 17: distribution of calcium in each lithofacies. MCcSt and Ccmt facies have the highest calcium content while the GS has the lower calcium content. 44

Figure 18: calcium distribution in each chemofacies. While the blue chemofacies have the highest calcium content, the yellow chemofacies has the lowest calcium content. 44

Figure 19: histogram for porosity and permeability in the Mississippian rocks. 45

Figure 20: linear relationship between porosity and permeability in Mississippian rocks. The highest porosity and permeability values correspond to CSt facies while the lowest values correspond to LMds. 45

Figure 21: box plot diagram showing the porosity distribution in each lithofacies. The CSt has the highest porosity values, while the bioturbated (BMdst) and laminated (LMdst) mudstones have the lower porosity values. 46

Figure 22: box plot showing the permeability distribution in each lithofacies. Only one sample was measured in each BMds and LMds. 47

Figure 23: cross plot between hardness (LH) and calcium (ppm). Hardness values were measured with the Equotip Picolo2 hardness tester and calcium (ppm) were measured with the HHXRF. 48

Figure 24: parameters used to evaluate the reservoir quality: lithofacies, total core gamma ray, total organic carbon (TOC), S2 peak, S1 peak, hardness data from the Equotip Picolo2 hardness tester, porosity and chemofacies. 50

Figure 25: isopach maps from 1) Woodford, 2) GRP1 and 3) from the top of GRP1 to the Unconformity which corresponds to the Meramec (MRMC). 52

Figure 26: paragenetic sequence of Mississippian strata in the Merge area 55

Figure 27: elements maps of sample Payne 003 at a depth of 8954 ft. A) Circular backscatter detector B) map of the elements: Na, K, Mg, Si, Al, Fe, Ti, Ca, Zr. C) calcium map D) silicon map E) aluminum map F) sodium map G) iron map H) magnesium map 58

Figure 28: correlation of carbon isotopes curves in the Merge area with two type curves, one in the Arrow Canyon Range (Batt et al., 2007; Saltzman, 2003) and one in the Anadarko basin (Koch et al., 2014). Three jumps were correlated: the jump between Devonian and Kinderhookian rocks, the jump between Osagean and Meramecian rocks and the jump within Chesterian rocks (not present in the Merge area). 61

LIST OF TABLES

Table 1: samples taken from Skaggs and Payne cores. . These samples were sent for a thin section, isotopic, and mineralogical composition (XRD) analysis. FP stands for feldspar and plagioclase..... 12

Table 2: nine selected variables with the paleoenvironmental interpretation. This set of elemental proxies (carbonate source, clay minerals, quartz, continentally-derived, and bottom water anoxia) were used to identify the chemofacies and interpret the conditions of deposition. 13

Table 3: correlation matrix between the nine original variables. Some variables show a direct correlation with a positive linear slope (e.g. Al vs K), inverse correlation with a negative linear slope (e.g. Ca vs Ti), or no correlation (e.g. Mo vs Si/Al). This correlation matrix is used to identify any correlation between the variables, a positive slope implies both variables are dependent between them, suggesting those variables share the same conditions of deposition. Negative slope implies both variables are dependent, but suggests the variables occur in different conditions of deposition. No correlation implies the variables are independent between them... 15

Table 4: principal component analysis (PCA). The original 9 variables were transformed into principal components, each original variable charges in different proportions the principal components. The cumulative proportion of each principal component is used to define the number of PCs used (PC3 in this case) to explain around 80% of the data variance. 16

Table 5: samples taken for porosity/permeability and organic richness analysis. 18

ABSTRACT

Historically, Mississippian rocks (Meramec / Sycamore Fms.) have been a productive oil and gas formations in Oklahoma. This study followed upon two major plays that were recently identified, The Sooner Trend Anadarko Canadian Kingfisher (STACK) play and the South-Central Oklahoma Oil Province (SCOOP) play. Few studies have been published about these plays, and even less is known about the Merge play, that as the name suggests is connection between the STACK and SCOOP plays. This study identified the factors that control the stratigraphy and reservoir quality of Meramec/Sycamore and Woodford strata to build a predictive sequence stratigraphic model.

Description of two cores, thin sections, scanning electron microscopy (SEM), and X-Ray fluorescence spectroscopy (XRF) were used for the identification, analysis, and interpretation of litho- and chemofacies. Differences in geologic factors like conditions of deposition, sediment source, and burial diagenesis resulted in two major facies associations: gravity flows, and hemipelagic sediments. Gravity flows are mainly massive (unstructured) calcite-cemented siltstones and hemipelagic facies are mainly laminated and bioturbated facies.

Porosity/permeability, hardness, TOC and rock-eval data were used to evaluate the range of reservoir quality and production potential of the two rock types. There are two main types of calcite in the facies, allochems and blocky calcite cement. In the gravity flow facies, blocky calcite cement precipitated during diagenesis and consequently occludes the original porosity but in the hemipelagic facies, calcite has not been precipitated thus it does not occlude the porosity. The amount of carbonate allochems controls the hardness of the rock in the hemipelagic facies, with more allochems resulting in harder rock.

Bulk-rock carbon and oxygen isotopic composition ($\delta^{13}C$ and $\delta^{18}O$) were used to interpret the origin of the blocky calcite cement and to build a relative time framework. The data suggest a marine bioclastic source of the carbonate from surrounding beds as the origin of the blocky calcite cement. Changes in the composition of the rock, in this case isotopic ($\delta^{13}C$) and elemental composition, were used to build a relative time framework and strengthen the sequence stratigraphic model. Based on this, it seems that the Mississippian/Pennsylvanian unconformity eroded the uppermost section of Mississippian strata in the Merge play.

While unconventional resources contain specific sweet spots and target zones, this integrated study demonstrates that geologic factors are still the path to quantifying and characterizing the rock potential.

An integrated study like this one depends on conditions of deposition, sediment source, and diagenesis -including distribution of the facies in the Merge play- and provided a chronostratigraphic framework, and a robust sequence stratigraphic model which provides a tool to interpret and predict genetically related depositional units in the available space. From this, sweet spots and anomalous zones could be detected.

1. INTRODUCTION

Historically, Mississippian rocks have been a productive oil and gas reservoir in the Anadarko basin. The operations are concentrated in two major plays: The Sooner Trend Anadarko Canadian Kingfisher (STACK) play and The South-Central Oklahoma Oil Province (SCOOP) play. Few studies have been completed for the Meramec Formation in the STACK, and the Sycamore Formation in the SCOOP (Huffman and Barker, 1950; Bennison, 1956; Curtis and Champlin, 1959; Braun, 1961; Culp, 1961; Peace, 1994; Franklin, 1997; Coffey, 2001; Miller, 2018; Milad and Slatt, 2018; Price et al. 2017), and even less is known for the connection of these two systems in the area recently named as the Merge play. Thus, understanding the geological factors (deposition and diagenesis) that affect the system helps to identify facies with high and low porosity and hardness values. The next pages refer to reservoir quality and production potential when talking about porosity and hardness of the rock since both factors are important when planning horizontal drilling and hydraulic fracture jobs.

Although previous authors defined these formations as limestones (Curtis and Champlin, 1959; Culp, 1961), recent studies (Price et al., 2017; Miller, 2018) have defined the systems as a mixed carbonate-siliciclastic system to differentiate it from the pure carbonate Osage limestone in the STACK play. Neither Osage limestone nor Chesterian aged rocks were found in the area under this study, thus, the mixed carbonate-siliciclastic system is referred to as Mississippian strata rather than using Meramec or Sycamore names.

This study focuses on understanding the geological factors that affect the production potential of Mississippian strata in the Merge play. By combining this reservoir characterization, and a chronostratigraphic framework in the STACK, Merge and SCOOP plays, one may build a sequence stratigraphic model to predict reservoirs with high and low quality. However, this study

focusses in the Merge area and not in the STACK and SCOOP plays, therefore it does not aim to understand the connection between the Meramec and Sycamore formations, but it gives an understanding of the undifferentiated Mississippian strata.

Even though the importance of this system is increasing among the Oil and Gas industry, few studies are completed regarding the reservoir quality in Mississippian strata (Price et al., 2017). The hydrocarbon generation, the storage capacity, and the brittleness of the rock are essential elements when targeting horizontal wells for the exploitation of unconventional resources. Assuming the Mississippian strata as a tight unconventional reservoir rather than a self-source reservoir, this study investigates what elements and processes affect the reservoir quality and hardness in the system. It is believed the amount of calcite controls the reservoir quality in this mixed carbonate-siliciclastic system and the type of calcite strongly affects the porosity and permeability of the rock. The system has diverse types of calcium carbonates. Siliciclastic depositional processes control the occurrence of the allochems, but diagenesis controls the occurrence of the calcite that cements the rock. Therefore, both the origin and distribution of the different carbonate elements are essential for reservoir characterization.

This study aims to evaluate what factors affect the porosity/permeability and hardness of the reservoir and the relation of these factors with deposition and diagenesis.

Chronostratigraphy is important when building a sequence stratigraphic model, hence a relative time framework has been built based on the idea that changes in the compositions of the rock can be related to changes during time. For example, changes in oxic-anoxic conditions and changes in sediment source can be identified in the elemental composition, or significant changes in the environment during depositions can be identified with carbon and oxygen isotopic composition ($\delta^{13}C$ and $\delta^{18}O$).

Therefore, combining stratigraphy, chemostratigraphy and a relative time framework, one may build a robust sequence stratigraphic framework that helps to predict the facies with high and low reservoir quality along the Anadarko basin.

2. GEOLOGICAL SETTINGS IN THE ANADARKO BASIN

2.1 Structural framework

The Anadarko basin, located in west-central Oklahoma, is bounded by the Wichita uplift to the south, the Amarillo-Wichita uplift to the west, the Arbuckle and Nemaha uplifts to the east, and the Anadarko shelf to the north. Three major tectonic events are related with the genesis of the Anadarko basin: rifting, passive margin development, and plate collision.

The first event is related to a three-arm rift or triple junction during the late Proterozoic to early Paleozoic. Two of these arms are associated with the opening of the Protoatlantic Ocean; the other arm failed and formed the Southern Oklahoma Aulacogen (SOA) (Ham et al., 1965; Burke and Dewey, 1973; Ham, 1978; Allen, 2000). Only the northern portion of the SOA formed the present Anadarko basin (Ham et al., 1965).

The second event is associated with subsidence and passive margin of the aulacogen. This controlled the deposition of a thick sedimentary sequence along an asymmetric foreland and the Anadarko shelf during early Cambrian to early Mississippian time (Lowe, 1975; Evans, 1979; Lane and De Keyser, 1980; Gutschick and Sandberg, 1983; Keller et al., 1983). In Mississippian time three major structures existed: Anadarko-Ouachita basin, the northern Oklahoma shelf, and the Ozark uplift. Then, North America and Gondwana collision triggered the Ouachita Orogeny forming major uplifts such as the Nemaha Ridge, Wichita and Arbuckle mountains, and major basins such as Marietta, Ardmore, and Anadarko (Ham et al., 1965; Feinstein, 1981; Perry, 1989).

2.2 Stratigraphy

Throughout Early Mississippian time (359-340 My.), a great part of North America was covered by an extensive, shallow, and tropical sea (Figure 1) (Ham, 1978; Gutschick and Sandberg, 1983; Blakey, 2013). To understand Early Mississippian strata in the Anadarko basin, it is essential to study the entire Mississippian units divided accordingly to the North American system. The Mississippian series is subdivided into four stages from older to younger: Kinderhookian, Osagean, Meramecian, and Chesterian (Figure 2).

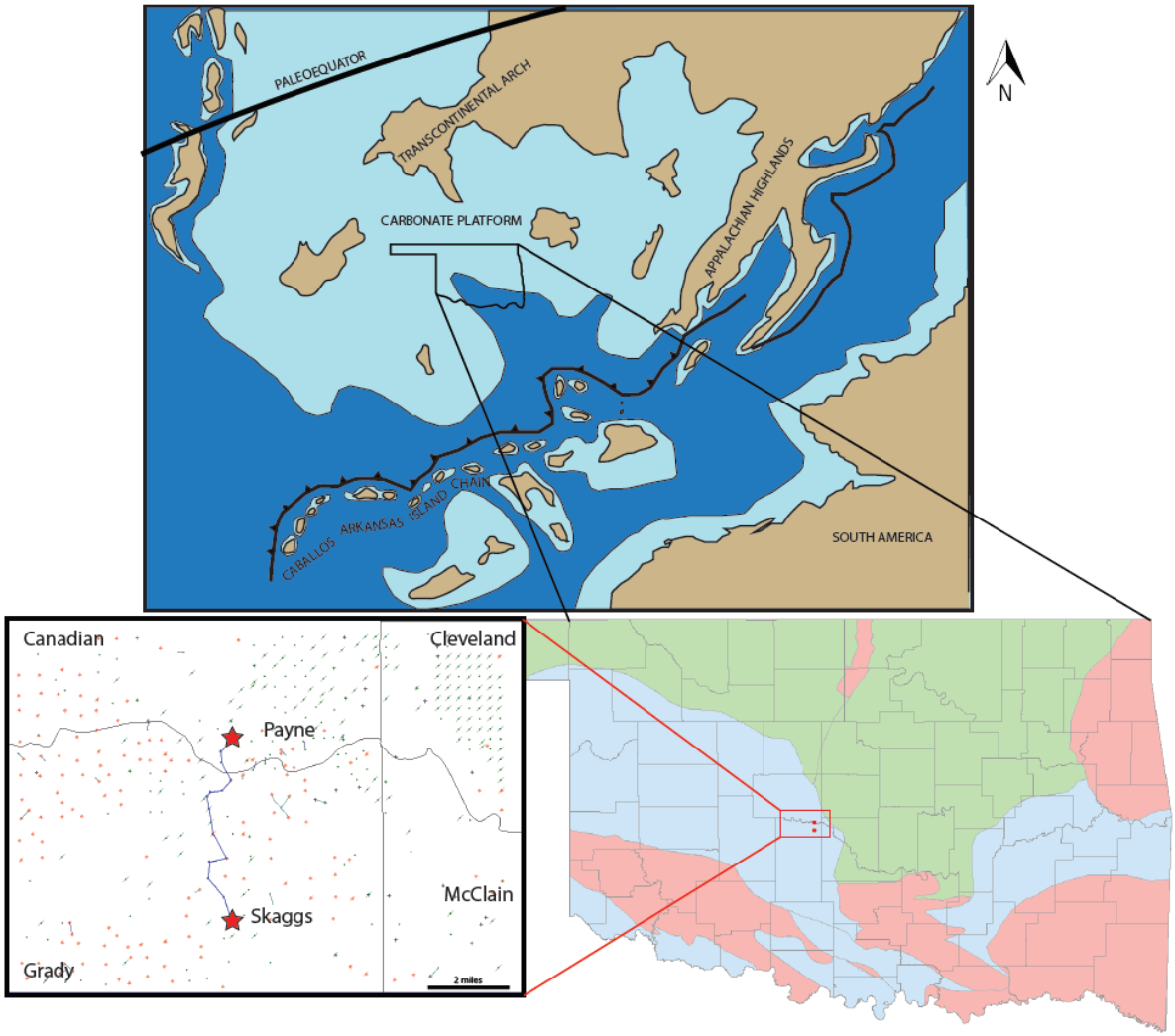

Figure 1: early Mississippian pelotopographic map and location map. It shows the location of the area of study in central Oklahoma. Geological provinces in Oklahoma (bottom right). Skaggs and Payne (red stars) cores located in Grady and Canadian counties (Anadarko basin),

respectively (bottom left). More than 800 wells, the green dots are oil wells and red dots are gas wells in the area of study from HIS databased (bottom left). Modified from Blakey, 2013; Gutschick and Sandberg, 1983

Global Series/Stage			North American Series/Stages			Curtis and Champlin, 1959		Peace, 1994			Culp, 1961	Bennison, 1956	Braun, 1961
						Lawrence Uplift	Anadarko basin	Sooner Trend Area	T 8N - 13N	T 6N - 7N	Anadarko Basin	Anadarko	Anadarko Basin
Carboniferous	Middle	Moscovian	Carboniferous	Pennsylvanian	Morrowan			Morrow	Morrow	Morrow			
		Bashkirian							Chester/ Springer	Springer			
	Lower	Serpukhovian		Mississippian	Chesterian	Canye	Chester	Chester			Caney	Caney/Chester	Caney
		Visean			Meramecian		Meramec	Osage-Meramec	Caney	Caney	Sycamore	Sycamore	Sycamore
					Osagean	hiatus	Osage		Sycamore	Sycamore	Osage or "Pre-Sycamore"	?	No deposition
		Tournaisian										Welden	
					Kinderhookian	Welden	Kinderhookian				Welden		Welden
Devonain	Upper	famenian	Devonian		Chattanoogan	Woodford	Woodford	Woodford	Woodford	Woodford	Woodford	Woodford	Woodford
		frasnian											

Figure 2 Mississippian stratigraphy from the Anadarko basin , based on different studies (Bennison, 1956; Braun, 1961; Culp, 1961; Curtis and Champlin, 1959; Peace, 1994).

During Kinderhookian time, the oldest stage, shallow and protected seas were close to the Caballos-Arkansas Islands chain (Gutschick and Sandberg, 1983). The formations for this stage are: Welden limestone (or “Pre-Sycamore”) in the Arbuckles, and Ardmore basin and Kinderhook in Anadarko basin (Curtis and Champlin, 1959). Some authors have placed the top of the Woodford in Kinderhookian time immediately underlying the Sycamore limestone (Bennison, 1956; Braun, 1961). Furthermore, a lower green shale is reported in south Oklahoma which marks the base of the Welden formation (Huffman and Barker, 1950; Braun, 1961; Culp, 1961).

Osagean rocks are truncated to the south by Meramecian units, suggesting an uplift related to the Ouachita orogeny. Welden limestone in the Lawrence uplift and Osage in the northern part of the Anadarko basin are placed in Osagean time (Bennison, 1956; Curtis and Champlin, 1959). In the

southern portion of the Anadarko basin, the thick Sycamore limestone is divided into an upper limestone and a lower cherty limestone with shale. The lower part is placed in the Osagean series and correlated in time with the upper portion of the reported Pre-Sycamore (Harlton, 1956).

In late Mississippian time, the Nemaha ridge experienced an uplift related to the Ouachita orogeny. Consequently, Meramecian units thin toward the north. General marine transgression and subsidence in late Mississippian time resulted in the deposition of the Sycamore and Meramec formations in the southern and northern portions of the Anadarko basin, respectively (Curtis and Champlin, 1959; Peace, 1994). Braun (1961) restricted the name Sycamore in the Ardmore and south Anadarko basin to the upper massive silty limestone of the Sycamore and proposed Meramecian age deposition (Bennison, 1956; Harlton, 1956; Braun, 1961; Culp, 1961). Finally, the thickness of Chesterian rocks (Caney, Goddard, and Chester) decreases towards the Nemaha ridge (Curtis and Champlin, 1959) due to Mississippian-Pennsylvanian tectonism.

Physicochemical conditions varied from the shelf in the north to the basin in the south, resulting in a variety of lithofacies that are difficult to correlate without a time-stratigraphic framework. Also, during Meramecian time the tectonic activity increased, raising a question about the source of the sediments. While provenance studies are needed to answer that question, based on geographical location the following possible sources are reasonable: Appalachian highlands and Ozark uplift in the northeast, transcontinental arch in the northwest, and the Caballos-Arkansas Island chain in the south. The two factors, physicochemical conditions and tectonism, resulted in lateral variations of facies, which makes the nomenclature of Mississippian units along Oklahoma more complex than expected (Figure 2).

3. METHODS AND MATERIALS

Two cores, Skaggs and Payne, separated six miles from each other were used to build one section of Mississippian strata in the Merge play. The Skaggs core has around 15 ft of the Devonian Woodford shale, the lower contact of Mississippian strata, and around 25 ft of Mississippian Rocks. The Payne core has around 65 ft of Mississippian units, around 3 ft of a major unconformity, and 1 ft of Pennsylvanian rocks. Therefore, combining both, Skaggs and Payne cores, this study analyzed 90 ft of Mississippian strata and around 15 ft of the Woodford shale (Figure 3). From the top of the Woodford to the upper unconformity in the Merge play, the thickness of Mississippian strata ranges between 150 and 120 ft.

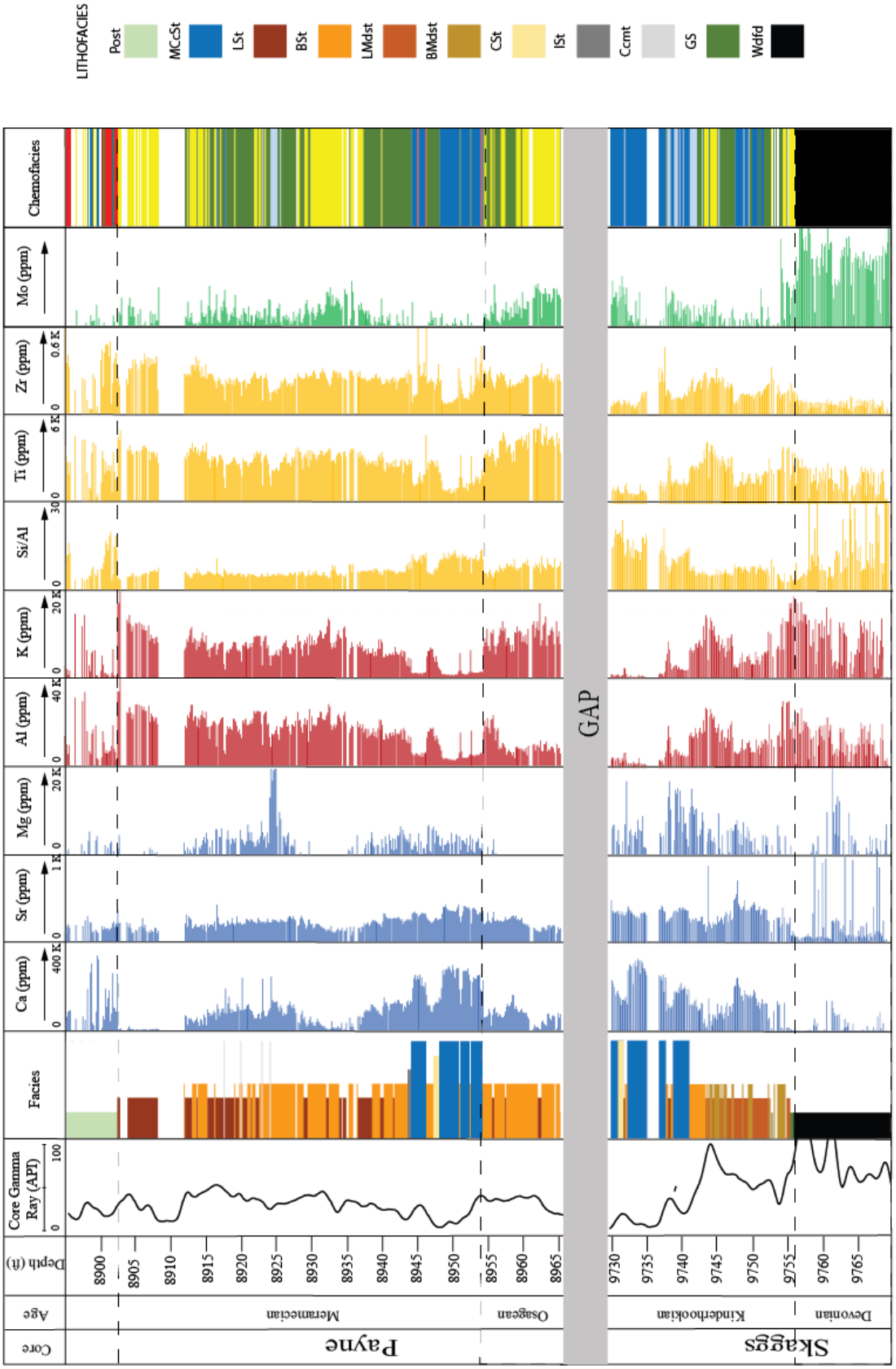
LITHOFACIES
Post
MCcSt
LSt
BSt
LMdst
BMdst
CSt
ISt
Ccmt
GS
Wdfd
Core
Age
Depth (ft)
Core Gamma Ray (API)
Facies
Ca (ppm)
Sr (ppm)
Mg (ppm)
Al (ppm)
K (ppm)
Si/Al
Ti (ppm)
Zr (ppm)
Mo (ppm)
Chemofacies
Payne
Skaggs
Meramecian
Osagean
Kinderhookian
Devonian
GAP

Figure 3: Skaggs and Payne cores profile with 2-inch vertical spacing; core gamma-ray, lithofacies, elemental composition and chemofacies. Lithofacies; Massive calcite-cemented siltstone (MCcSt), Calcareous siltstone (CSt), Bioturbated siltstone (BSt), Laminated siltstone (LSt), Bioturbated mudstone (BMdst), Laminated mudstone (LMdst), Interbedded siltstone (ISt), calcite cement (Ccmt), strata around the unconformity (Post), glauconitic sandstone (GS), and Woodford shale (Wdfd).Chemofacies are related with the elemental composition in the following manner: blue chemofacies with high Calcium and Strontium; light blue with high Mg; red with high Si/Al and Zr; Green and Yellow chemofacies are distributed in low calcite-cemented lithofacies with similar elemental composition but differ in that yellow chemofacies has slightly more Ti, K, and Al, and the green chemofacies has more Molybdenum.

3.1. Petrographic analysis

The two cores located in the Merge play were described with two-inch vertical spacing (Figure 3). Core-plug samples were taken for further analysis. A total of thirty-three uncovered thin sections were taken and colored with K stain for calcite identification. Grain size, sorting, structures, cement, and fossils were described using a Zeiss AxioImager Z1TM petrographic microscope.

From the 33 samples, 13 samples were chosen to conduct scanning electron microscopy (SEM) to support petrographic observations of the microfabric. The 13 thin sections were covered with gold and examined under the SEM (FEI Quanta 250) with a coupled Bruker Electron Spectrometer (EDS). Microphotographs were taken using both Everhart Thornley Detector (ETD) and Circular backscatter detector (CBS) at the following operation conditions: working distance (WD) 15 mm and accelerating voltage (HV) 25 keV.

3.2. Isotopic analysis (δ^{13}C‰ and δ^{18}O‰)

Carbon and oxygen isotopes of whole-rocks were analyzed to interpret the origin of the waters that helped to precipitate the calcite cement. One milligram of each of the 33 samples (Table 1), was sent to Keck-NSF Paleoenvironmental and Environmental Laboratory at the University of Kansas for the isotopic analysis. A ThermoFinnigan GasBench II in-line with a Finnigan MAT 253 isotope-ratio mass spectrometer was used for the analysis with ±0.12‰ and±0.06‰ precision for oxygen and carbon, respectively. The results are presented in δ^{13}C ‰ based on Vienna PeeDee Belemnite (VPDB) standards.

3.3. X-Ray diffraction

In this study, 20 samples (Table 1) were prepared and analyzed for X-Ray diffraction spectroscopy. Each sample was pulverized, dried, and mounted on glass holders following procedures described in the Laboratory Manual by Madden (2011). The Rigaku Ultima IVTM diffractometer was used to collect the diffraction patterns and then the MDI Jade 2010 software was used to interpret these patterns.

Table 1: samples taken from Skaggs and Payne cores. . These samples were sent for a thin section, isotopic, and mineralogical composition (XRD) analysis. FP stands for feldspar and plagioclase.

Core	Depth	Lithofacies	d ^{13}C VPDB	d ^{18}O VPDB	Quartz	FP	Calcite	Dolomite/ Ankerite	Muscovite	Clays	Pyrite
	ft		‰	‰	%	%	%	%	%	%	%
Payne	8895.0	Post	-5.10	-7.17	77	3	16	1	2	1	0
Payne	8898.0	Post	-4.20	-5.29	6	0	78	1	1	13	0
Payne	8901.0	Post	-4.12	-7.60	75	1	20	1	1	1	0
Payne	8913.0	BSt	-2.18	-4.42	61	10	5	5	17	1	1
Payne	8918.0	LSt	-1.25	-2.63	-	-	-	-	-	-	-
Payne	8919.0	BSt	-0.54	-2.78	-	-	-	-	-	-	-
Payne	8921.0	BSt	-1.08	-3.11	-	-	-	-	-	-	-
Payne	8922.0	LSt	0.32	-2.20	-	-	-	-	-	-	-
Payne	8924.0	BSt	-1.62	-2.87	-	-	-	-	-	-	-
Payne	8926.0	BSt	-0.06	-3.15	-	-	-	-	-	-	-
Payne	8930.0	BSt	0.67	-2.62	-	-	-	-	-	-	-
Payne	8938.0	BSt	0.34	-2.72	-	-	-	-	-	-	-
Payne	8940.0	Ccmt	-2.65	-4.73	26	5	59	6	4	0	0
Payne	8941.0	LSt	1.10	-2.83	36	8	19	17	14	6	1
Payne	8942.0	BSt	0.55	-2.72	39	7	21	14	16	2	1
Payne	8943.0	MCcSt	-0.19	-4.42	30	5	58	1	1	4	1
Payne	8947.0	CSt	-1.26	-2.65	44	8	19	18	8	3	0
Payne	8952.0	BSt	-0.56	-3.30	36	9	12	19	12	12	1
Payne	8954.0	MCcSt	-0.71	-4.47	33	5	54	3	5	0	1
Payne	8957.5	BSt	-0.34	-3.18	-	-	-	-	-	-	-
Payne	8958.5	BMds	-0.20	-2.65	40	9	14	9	20	7	1
Skaggs	9731.0	MCcSt	0.65	-3.13	48	4	36	10	2	0	0
Skaggs	9737.5	MCcSt	0.44	-3.44	24	4	60	7	4	0	0
Skaggs	9738.8	LSt	-0.60	-2.34	-	-	-	-	-	-	-
Skaggs	9741.0	MCcSt	0.28	-4.11	34	4	38	13	3	7	0
Skaggs	9742.8	LMds	-0.26	-2.70	47	5	14	13	19	0	1
Skaggs	9743.7	BMds	0.15	-3.08	-	-	-	-	-	-	-
Skaggs	9744.9	BMds	-1.15	-3.74	42	12	8	12	20	4	1
Skaggs	9747.5	BMds	-0.39	-2.33	41	3	22	13	16	2	4
Skaggs	9748.0	LMds	-	-	-	-	-	-	-	-	-
Skaggs	9749.0	BMds	-0.33	-3.84	-	-	-	-	-	-	-
Skaggs	9750.3	LMds	-0.45	-3.88	32	4	39	15	8	0	1
Skaggs	9755.5	Wdfd	-4.75	-5.00	31	10	2	2	41	13	1

3.3 Elemental composition from X-ray fluorescence spectroscopy

Each core was cleaned with water to avoid misreading caused by external contaminants like drilling mud. The Bruker Traces IV-SD hand-held X-ray fluorescence (HHXRF) spectrometer was used to measure the elemental composition of the rock. Major and trace elements were measured at a two-inch vertical spacing at the same point as the core description. Major elements were scanned under vacuum at 15 kV accelerating voltage for 90 seconds, then, trace elements

were analyzed under atmospheric pressure with a Ti-Al filter at 40 kV accelerating voltage for 60 seconds.

The resulting data was transformed to parts per million (ppm) using fundamental parameters (FP) for mudrocks in Rowe et al., 2012a. Out of 29 elements measured from the HHXRF, only 9 variables were used: eight elements (Table 2) and one ratio (Si/Al), which provide a set of carbonate proxies, clay proxies, continental input proxies, and bottom water marine anoxia proxies. The proxies were chosen based on the literature as proxies for carbonate source, clay minerals, quartz, continentally derived and bottom water anoxia (Turner et al., 2016; Algeo and Rowe, 2012; Rowe et al., 2012b; Tribovillard et al., 2006; Sageman and Lyons, 2004;), and because their uses helped to refine a sequence stratigraphic framework and to improve their level of understanding of this specific mixed carbonate-siliciclastic system.

Table 2: nine selected variables with the paleoenvironmental interpretation. This set of elemental proxies (carbonate source, clay minerals, quartz, continentally-derived, and bottom water anoxia) were used to identify the chemofacies and interpret the conditions of deposition.

Elemental Proxy	Paleoenvironmental Interpretation
Calcium (Ca)	Carbonate source
Strontium (Sr)	Carbonate source
Magnesium (Mg)	Dolomite source
Aluminum (Al)	Clay minerals and feldspars
Potassium (K)	Clay minerals and feldspars
Si/Al	Quartz
Titanium (Ti)	Continentally derived
Zirconium (Zr)	Continentally derived
Molybdenum (Mo)	Bottom water anoxia

3.4 Determination of chemofacies based on cluster analysis

Analogous to the lithofacies, the chemofacies are rock units characterized by a signature in the chemical composition. I identified these chemofacies by clustering rock samples with similar elemental composition. The purpose of clustering the data was to detect similarities and anomalies in the elemental composition that could not be attributed to the lithofacies. K-means algorithm (Hartigan and Wong, 1979) with Euclidean distance was used to group the data. For this algorithm, the optimal number of clusters and the elements (Table 2) are the inputs.

Two methods were used to define and validate the optimal number of clusters (chemofacies): average Silhouette method and Elbow method. Silhouette method (Rousseeuw, 1986) determines how well an object lies within its cluster, whereas the Elbow method describes how the variance changes with the number of clusters. The optimal number of clusters in the Elbow method is chosen where the inflection point separates the number of clusters that significantly increases the variance in the data from the number of clusters which does not significantly change variance. Therefore, Elbow method was the primary tool to select the optimal number of clusters, while the Silhouette method was used to validate the clusters in the data.

Prior Principal Component Analysis (PCA) (de Lima and Marfurt, 2018, 2018; Milad et al., 2018; Milad and Slatt, 2018) was used to describe the statistical importance of the variables (proxies) in each cluster, and based on the correlation matrix (Table 3) one may concluded there is correlation between the variables.

Table 3: correlation matrix between the nine original variables. Some variables show a direct correlation with a positive linear slope (e.g. Al vs K), inverse correlation with a negative linear slope (e.g. Ca vs Ti), or no correlation (e.g. Mo vs Si/Al). This correlation matrix is used to identify any correlation between the variables, a positive slope implies both variables are dependent between them, suggesting those variables share the same conditions of deposition. Negative slope implies both variables are dependent, but suggests the variables occur in different conditions of deposition. No correlation implies the variables are independent between them.

	Mg	Al	K	Ca	Ti	Sr	Zr	Mo	Si.Al
Mg	1.00	-0.09	-0.25	0.38	-0.32	0.32	-0.26	-0.16	0.03
Al	-0.09	1.00	0.78	-0.74	0.64	-0.52	0.24	0.13	-0.75
K	-0.25	0.78	1.00	-0.81	0.86	-0.54	0.19	0.35	-0.70
Ca	0.38	-0.74	-0.81	1.00	-0.82	0.69	-0.40	-0.37	0.56
Ti	-0.32	0.64	0.86	-0.82	1.00	-0.64	0.46	0.27	-0.57
Sr	0.32	-0.52	-0.54	0.69	-0.64	1.00	-0.43	-0.30	0.36
Zr	-0.26	0.24	0.19	-0.40	0.46	-0.43	1.00	-0.16	-0.09
Mo	-0.16	0.13	0.35	-0.37	0.27	-0.30	-0.16	1.00	-0.05
Si.Al	0.03	-0.75	-0.70	0.56	-0.57	0.36	-0.09	-0.05	1.00

After assuming there is a correlation between the variables (Table 3), principal component analysis (PCA) was performed for the reduction of dimensions. PCA uses an orthogonal transformation to convert the nine variables into principal components (PCs), and each original variable loads in the new variables (Table 4). Therefore, I used fewer variables to identify the elemental composition signature of each chemofacies.

Table 4: principal component analysis (PCA). The original 9 variables were transformed into principal components, each original variable charges in different proportions the principal components. The cumulative proportion of each principal component is used to define the number of PCs used (PC3 in this case) to explain around 80% of the data variance.

	PC1	PC2	PC3	PC4	PC5	PC6	PC7	PC8	PC9
Mg	0.170	-0.558	-0.233	0.752	-0.104	0.116	-0.046	-0.105	-0.047
Al	-0.383	-0.289	-0.191	-0.051	0.170	-0.449	-0.504	0.379	0.321
K	-0.419	-0.199	0.066	-0.121	-0.282	0.296	-0.124	0.336	-0.686
Ca	0.428	-0.062	-0.079	-0.031	0.059	0.077	0.364	0.809	0.094
Ti	-0.419	0.070	-0.033	0.060	-0.363	0.534	0.130	0.072	0.613
Sr	0.347	-0.241	-0.070	-0.362	-0.769	-0.250	-0.115	-0.102	0.095
Zr	-0.198	0.555	-0.447	0.350	-0.323	-0.391	0.188	0.112	-0.161
Mo	-0.157	-0.054	0.800	0.307	-0.189	-0.374	0.213	0.114	0.068
Si.Al	0.327	0.434	0.230	0.253	-0.121	0.226	-0.697	0.191	0.019
Standard deviation	2.172	1.142	1.083	0.823	0.638	0.529	0.495	0.363	0.253
Proportion of Variance	0.524	0.145	0.130	0.075	0.045	0.031	0.027	0.015	0.007
Cumulative Proportion	0.524	0.669	0.799	0.875	0.920	0.951	0.978	0.993	1.000

3.5 Sequence stratigraphy

Sequence stratigraphy subdivides the sedimentary sequence into genetically-related sediments bounded by key surfaces, such as sequence boundaries, maximum flooding surfaces, and correlative conformities. Changes in the sedimentation rates and the accommodation space of the basin generate these surfaces, resulting in changes of the relative sea level position.

I identified key surfaces -flooding surfaces and regressive surfaces- based on core description and gamma ray log by looking peaks and troughs in the radioactive response of the rock. Then, I identified parasequence stacking patterns or Gamma Ray Parasequences (GRP) by recognizing the trends of increasing-upward or decreasing-upward gamma ray counts. After the interpretation of key surfaces and stacking patterns, the depositional sequences were interpreted using the core

description and elemental composition from the HHXRF to build a robust sequence stratigraphic framework.

3.6 Organic geochemistry

51 samples were used to measure total organic content (Leco-TOC) and Rock-Eval pyrolysis (S1, S2, Tmax) (Table 5) to evaluate the organic richness and to interpret reservoirs and productive intervals within Mississippian strata. The parameters I used to evaluate the organic richness are:

TOC = total organic carbon found in the sample

S1 = the amount of free residual hydrocarbon content (gas and oil) in the sample

S2 = the amount of hydrocarbon generated through thermal cracking of non-volatile organic matter

Table 5: samples taken for porosity/permeability and organic richness analysis.

Core	Depth ft	Lithofacies	Chemofacies	Porosity %	Permeability Md	LECO TOC wt%	S1 mg HC/g	S2 mg HC/g	Tmax ˚C
Payne	8895.0	Post	Red	3.73	0.00100	0.65	0.59	1.41	438
Payne	8898.0	Post	Green	2.46	0.00400	0.63	0.00	0.03	403
Payne	8901.0	Post	Red	-	-	0.40	0.03	0.10	373
Payne	8913.0	BSt	Yellow	5.6	0.00100	1.03	0.35	1.97	440
Payne	8918.0	LSt	Green	1.8	0.03700	1.96	0.60	5.00	441
Payne	8919.0	LSt	Green	3.97	0.01200	0.95	0.29	1.59	439
Payne	8921.0	BSt	Green	3.95	0.00100	0.73	0.30	1.58	441
Payne	8922.0	LSt	Yellow	3.02	0.12100	0.70	0.70	1.48	439
Payne	8924.0	BSt	LightBlue	2.23	0.00008	0.83	0.38	1.62	442
Payne	8926.0	BSt	Green	1.97	0.00008	0.76	0.28	1.65	439
Payne	8930.0	BSt	Yellow	4.27	0.00300	1.60	0.76	5.35	439
Payne	8938.0	BSt	Green	4.05	0.00100	1.07	0.99	3.94	441
Payne	8940.0	BSt	Green	1.95	0.00020	0.87	0.31	1.93	436
Payne	8941.0	BSt	Green	2.36	0.00009	0.71	0.90	2.30	442
Payne	8942.0	BSt	Green	3.97	0.00040	0.42	0.36	0.63	438
Payne	8943.0	BSt	Green	6.12	0.00600	1.36	0.63	2.56	443
Payne	8947.0	CSt	Green	9.31	0.02900	1.76	0.70	5.60	442
Payne	8952.0	BSt	Green	6.86	0.00500	0.85	0.81	1.77	439
Payne	8954.0	MCcSt	Green	-	-	0.16	0.48	0.81	427
Payne	8957.5	BSt	Green	4.08	0.06100	0.16	0.32	1.19	439
Payne	8958.5	BMds	Green	0.65	0.00005	1.64	1.70	4.06	442
Skaggs	9731.2	CSt	Blue	9.74	0.05000	0.45	-	-	-
Skaggs	9732.2	BSt	Blue	2.01	0.00020	0.33	-	-	-
Skaggs	9734	MCcSt	Blue	3.71	0.00800	0.30	-	-	-
Skaggs	9735.2	MCcSt	Blue	3	0.00030	0.41	-	-	-
Skaggs	9736.1	BSt	Blue	5.62	0.00300	0.61	-	-	-
Skaggs	9737.8	MCcSt	Blue	2.85	0.00020	0.83	-	-	-
Skaggs	9740.4	CSt	Blue	6.36	0.00200	0.79	-	-	-
Skaggs	9741.3	BSt	LightBlue	3.01	-	0.80	-	-	-
Skaggs	9743.2	LMds	Yellow	0.23	0.00004	0.88	-	-	-
Skaggs	9744.2	BMds	Green	2.34	-	0.99	-	-	-
Skaggs	9745.7	BMds	Green	0.46	-	1.13	0.63	2.99	444
Skaggs	9746.8	LMds	Green	0.27	-	0.88	-	-	-
Skaggs	9747.8	LMds	Green	0.21	-	1.50	0.93	6.08	440
Skaggs	9748.8	LMds	Blue	0.6	-	1.09	1.38	4.85	437
Skaggs	9749.7	BMds	Blue	0.21	-	1.22	0.77	3.51	443
Skaggs	9750.8	LMds	Blue	0.27	-	1.26	0.69	3.41	443
Skaggs	9751.2	LMds	Blue	0.19	-	1.28	0.78	3.66	445
Skaggs	9753	BMds	Green	0.46	-	1.49	0.76	4.44	444
Skaggs	9754	BMds	Yellow	0.26	-	1.24	0.87	3.88	444
Skaggs	9756.4	Wdfd	Wdfd	1.4	-	0.46	-	-	-
Skaggs	9757.5	Wdfd	Wdfd	0.38	-	2.91	1.71	11.22	450
Skaggs	9758.6	Wdfd	Wdfd	0.31	-	3.84	2.49	14.42	446
Skaggs	9759.6	Wdfd	Wdfd	0.41	-	3.39	2.25	14.19	450
Skaggs	9760.4	Wdfd	Wdfd	0.4	-	5.33	3.03	23.85	445
Skaggs	9761.8	Wdfd	Wdfd	0.64	-	0.34	-	-	-
Skaggs	9762.9	Wdfd	Wdfd	2.91	-	6.27	3.84	23.43	447
Skaggs	9764.4	Wdfd	Wdfd	1.17	-	5.79	3.53	22.77	448
Skaggs	9765.4	Wdfd	Wdfd	0.31	-	2.25	1.77	7.28	446
Skaggs	9766.4	Wdfd	Wdfd	1.17	-	4.17	2.82	17.44	448
Skaggs	9768.4	Wdfd	Wdfd	0.84	-	2.97	2.12	10.63	446

3.7 Porosity/Permeability

Conventional plug analysis was run on 49 samples (Table 5) by Core Lab using CMS™-300 Core Measurement System and following conventional plug analysis procedure. Before measuring poro/perm, samples were dried at 240° F (115.5^{o}C) to weight equilibrium. Porosity was determined using Boyle's Law technique of measuring grain volume (ambient conditions) and pore volume at 4500 (psi) net confining stress (Jones, 1988). Only 27 samples were measured because the porosity in the lowermost section is below the detection limit of the equipment Klinkenberg Permeability (equivalent non-reactive liquid permeability). Values greater than 0.1 mD were measured using helium gas, whereas nitrogen gas was used for permeability values lower than 0.1 mD.

3.8 Rock hardness (micro-Rebound hammer)

The hardness of the rock was measured with a non-destructive Equotip Picolo^{2}. Based on the ratio between the rebound velocity and the impact velocity, this tool uses Leeb Hardness values (LH) (Leeb, 1979) as shown in equation 1. Average values were calculated from five measurements taken in the same point as core description and elemental composition.

$$1)\ \text{Hardness (LH)} = \frac{\text{Rebound velocity (Vr)}}{\text{Impact velocity (Vi)}} * 1000$$

3.9 Mapping

I generated isopach maps based on more than 800 well to identify the relationship between the Woodford shale and Mississippian strata. Starting from the core, I correlated key surfaces

through the area of study, such as the unconformable contact between the Hunton and the Woodford, the top of the Woodford, the top of the GRP1 (Kinderhookian age rocks), and the unconformity at the top of the Mississippian rocks.

4. RESULTS

4.1 Petrology

The diagenetic analysis uses petrography to understand the origin of the calcite cement and its effect on the porosity. The petrographic analysis concluded that the mixed carbonate-siliciclastic system of the Mississippian rocks are mainly siltstones composed of angular quartz grains with calcareous cement. Two big groups of lithofacies were determined based on the mineralogical composition. The first group contains a high content of calcite cement (>30%) and low clay content: Calcite cement (Ccmt) and Massive calcite-cemented peloidal siltstone (MCcSt). The second group is composed of lithofacies with low calcite cement (<30%) content, including bioturbated siltstone (BSt), laminated siltstone (LSt), interbedded siltstone (ISt), calcareous siltstone (CSt), bioturbated mudstone (BMdst) and laminated mudstone (LMdst). The more abundant facies in the Skaggs core are MCcSt, BMdst and LMdst whereas in the Payne core the most abundant facies are: MCcSt, BSt and LSt (Figure 3 & 4). It is worth stating that laminated lithofacies (LSt and LMdst) groups laminated and massive siltstones to differentiate from their bioturbated counterpart (BSt and BMdst).

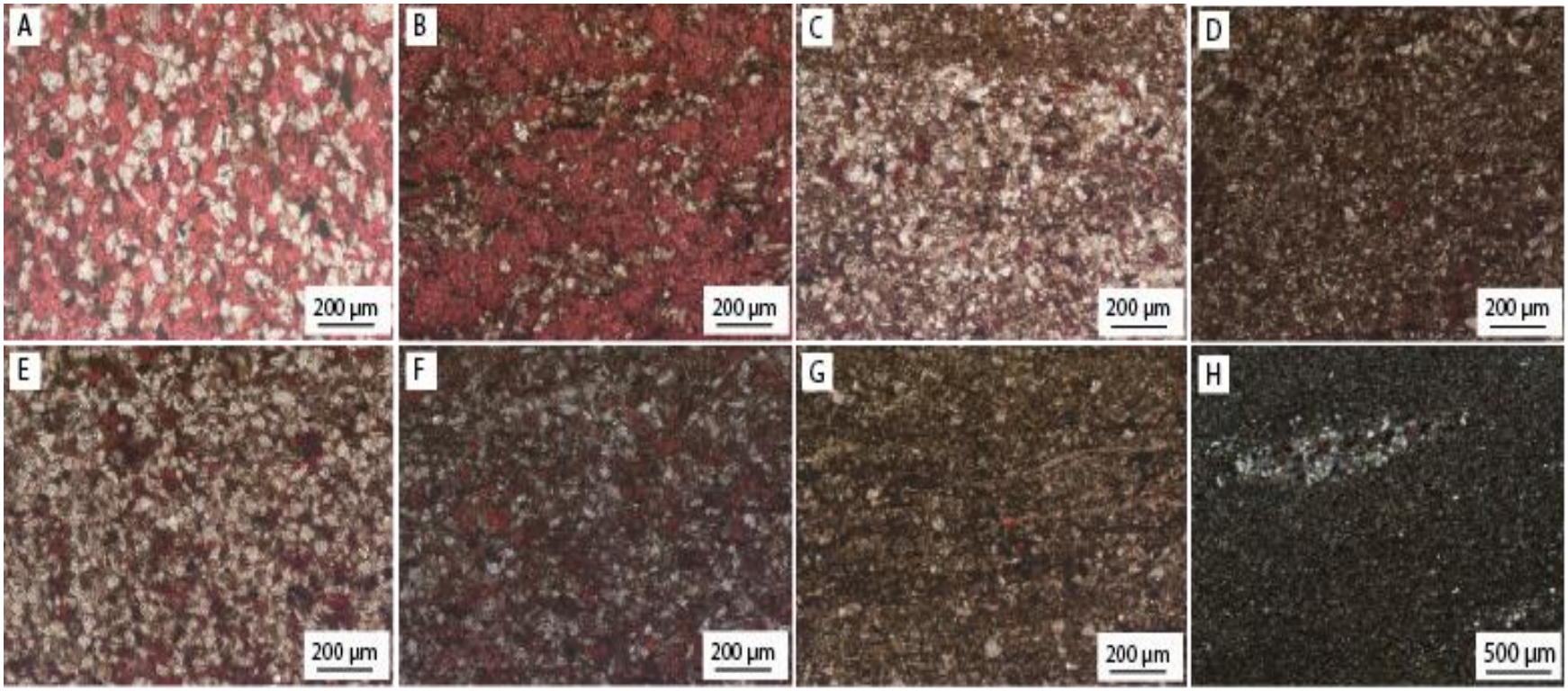

Figure 4: thin section photos from the facies found in Mississippian strata. A) massive calcite cemented siltstone (MCcSt) B) calcite cement (Ccmt) C) bioturbated siltstone (BSt) D) laminated siltstone (LSt) E) calcareous siltstone (CSt) F) Bioturbated mudstone (BMdst) G) laminated mudstone (LMdst) H) Interbedded siltstone (ISt)

From the core description, one foot of glauconitic sandstone (GS) was identified at the contact between the Woodford shale and overlying Mississippian rocks (Figure 3 & 5). The sample is mainly glauconite grains of very fine sand and smaller silty quartz grains. Also, a major unconformity (Figure 3, 6) was identified at the top of the section, where three samples were taken: two below the unconformity and one above it. For practical purposes, all three samples are named "Post" (Table 1 & 5) (Figure 3, 6).

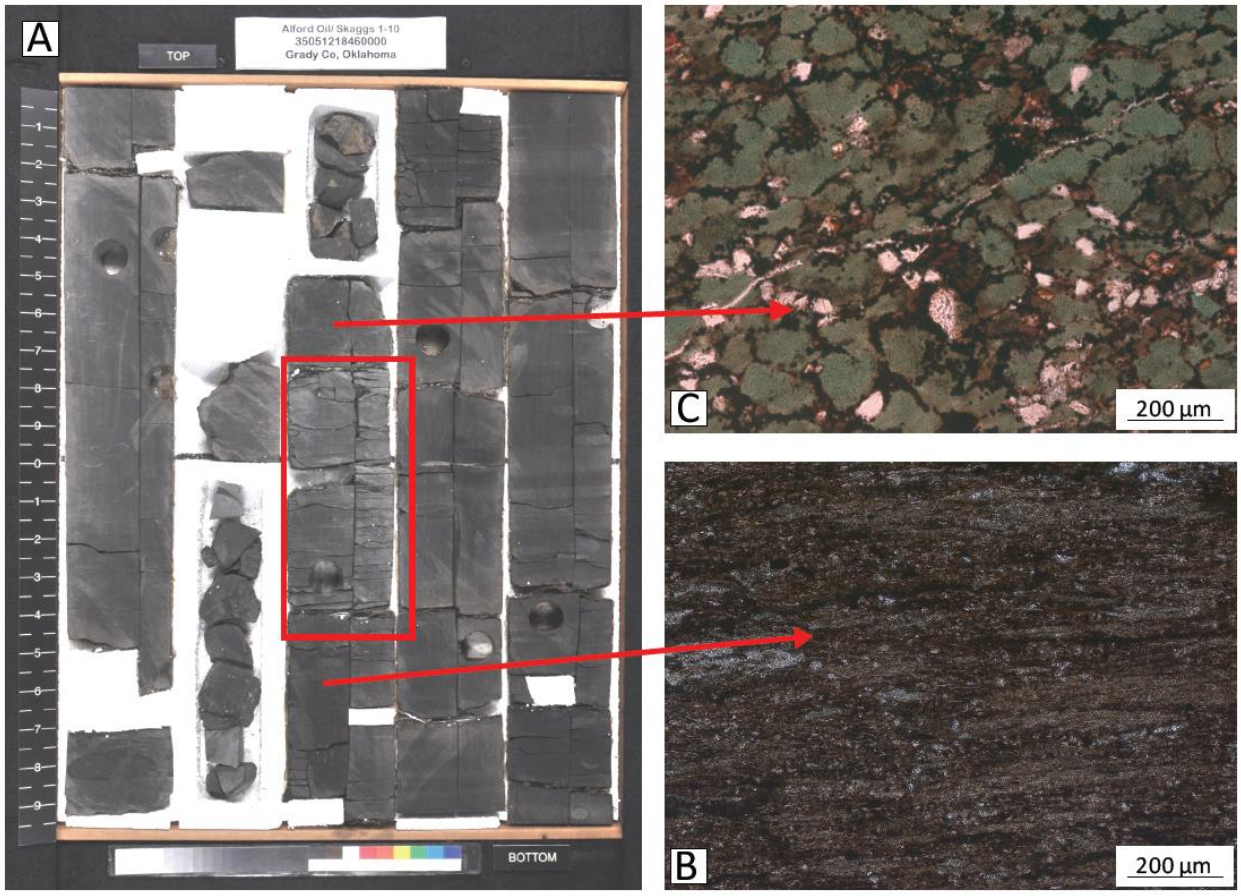

Figure 5: contact between the Woodford shale and Mississippian strata. A) core (Skaggs) photo of the contact. B) thin section photo of the Woodford shale below the unconformity. C) thin section photo of the glauconitic sandstone (GS) in the Mississippian rocks overlying the Woodford shale.

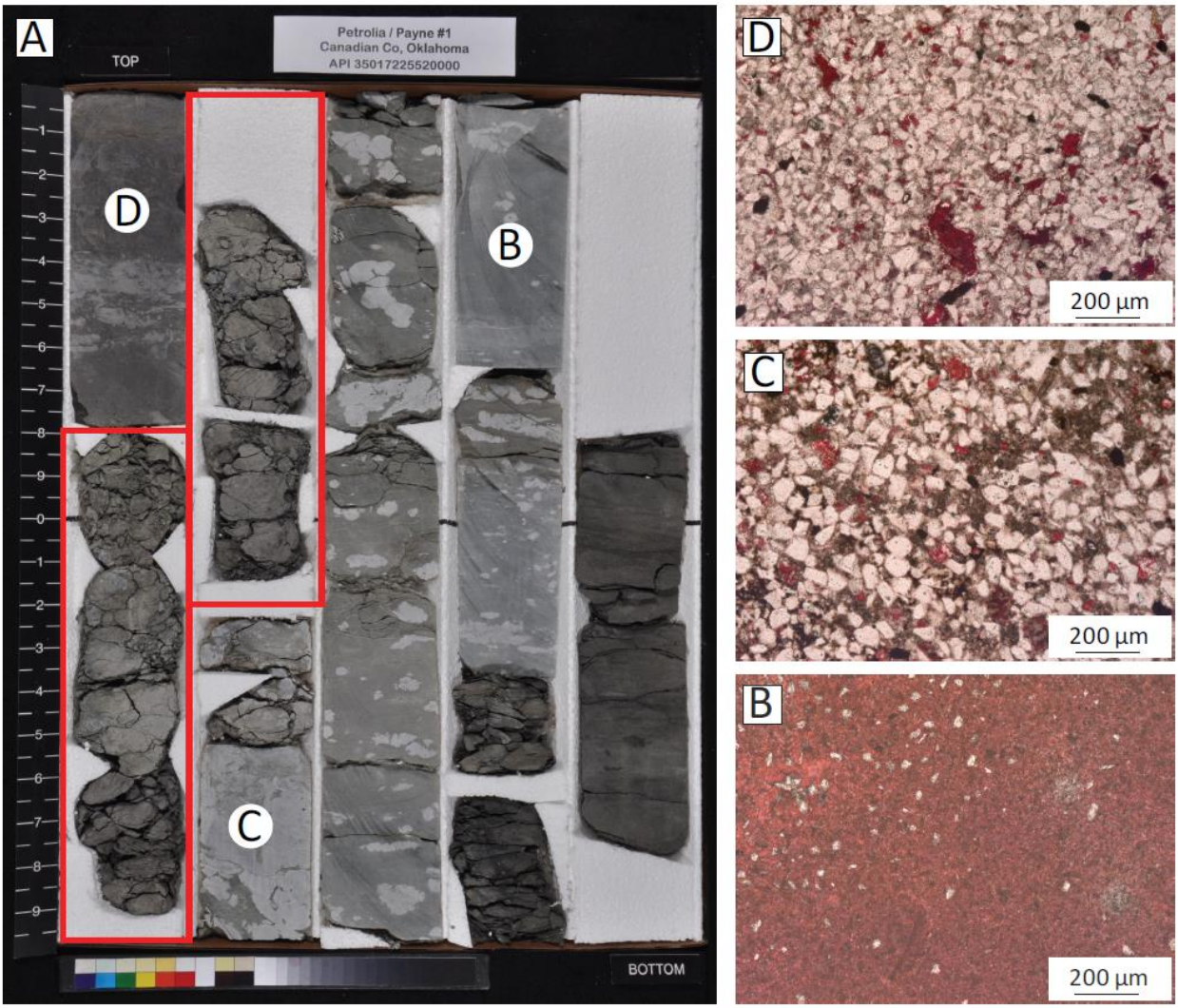

Figure 6: Mississippian/Pennsylvanian contact. A) core (Payne) photo of the contact with the location of the thin sections to the right. B) thin section photo of the Silty micrite at 8901 ft. C) Sparitic siltstone at 8898 ft. D) quartz-rich fine sandstone at 8895 ft. For future reference in the isotopes analysis, samples B, C and D are named "Post".

4.1.1. Detrital composition

The MCcSt facies has well-sorted grains presenting mainly floating texture (Figure 4A & 7) and point contacts but rarely concave/convex contacts. The main constituent in this facies are subangular to angular quartz, from very fine sand to medium silt size between 20 µm and 100 µm (silt size) (Figure 4A & 7). Quartz grains are monocrystalline with very few exceptions of polycrystalline grains presenting corroded texture and embayment boundaries where the grain is

in contact with calcite cement. Quartz overgrowths are not common in any of the samples analyzed. Feldspars grains are mainly plagioclase and they are less common than quartz grains in the MCcSt facies (Figure 7). Plagioclase is replaced and altered by calcite cement almost completely in some cases. Calcareous peloids are abundant in the MCcSt facies and are recognized because those are rod-shaped and stained deep pink (Figure 5 & 7). These peloids are composed of micrite (fine-grained calcite) with no internal structure and ellipsoidal shape. In some parts, the peloids show concave/convex contacts with the quartz. Other detrital constituents of the MCcSt facies are micas (mainly muscovite), calcareous rock fragments, and the heavy minerals: zircon ($ZrSiO_4$), pyrite (FeS_2), and rutile (TiO_2).

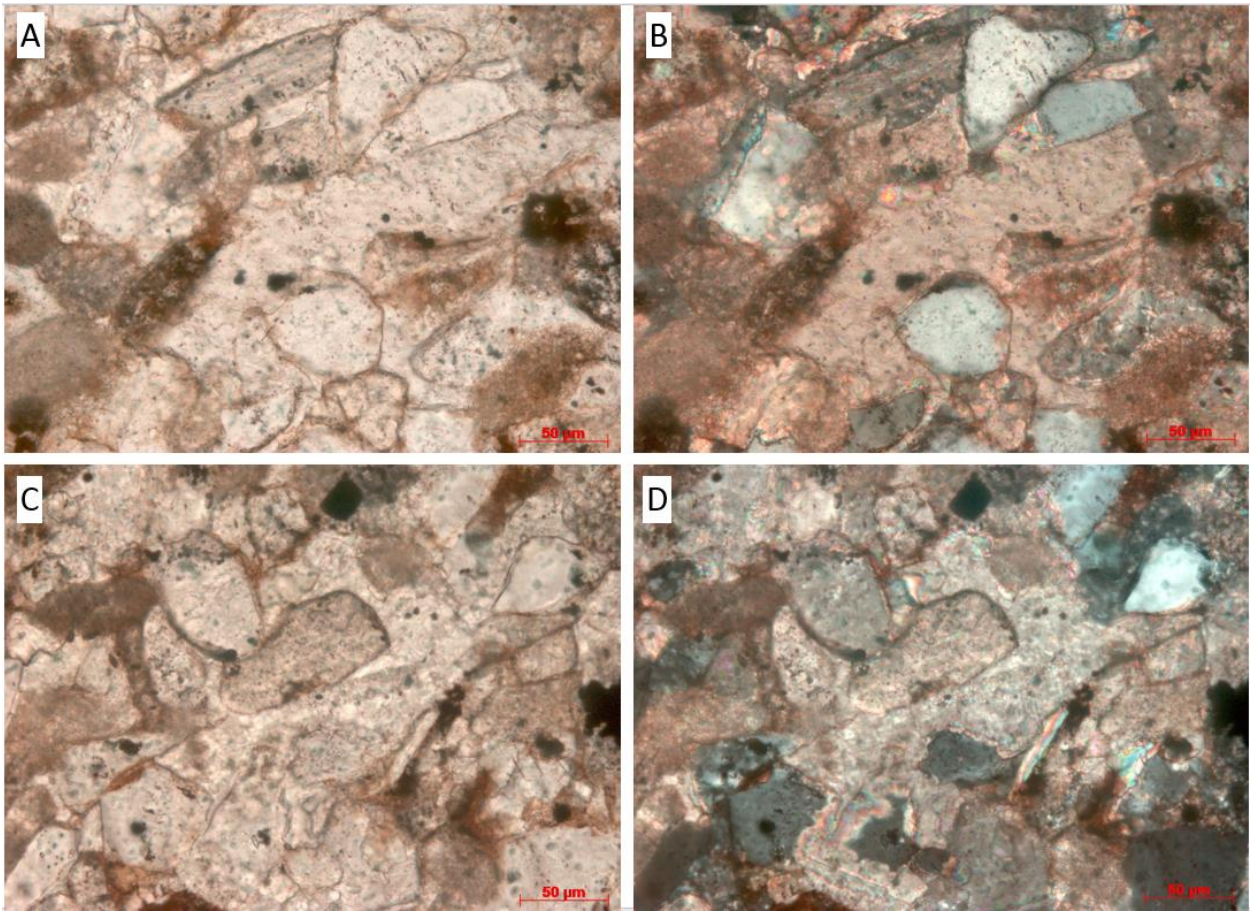

Figure 7: Petrographic photos of the Massive calcite-cemented siltstones (MCcSt). A) sample Payne 015 at depth 8942.0, parallel Nicols B) crossed Nicols C) sample Payne 003 at depth 8954.0, parallel Nicolls D) crossed Nicolls.

In the lithofacies with low calcite (< 30%) and high clay content, the major constituent is quartz grains from very fine silt to coarse silt grain size, averaging medium silt-size. Well-preserved fossils from 100 µm to 2 cm long are predominantly brachiopods (Figure 4C-4H). Other detrital constituents are feldspars, clays, rock fragments, and glauconite grains.

4.1.2. Diagenetic minerals and cements

Calcite cement is the main diagenetic mineral, but quartz cement, clays, pyrite, and Fe-oxides are also present in the rocks. Diagenetic calcite occurs primarily as blocky cement, engulfing and altering silicates in the MCcSt facies (Figure 7), but it also occurs as late unidirectional flows of calcite cement also referred to as secondary calcite cement (Ccmt) (Figure 4B). The blocky calcite cement is producing the floating texture, and its up to 400 µm crystals occludes the porosity, as well as dissolves and alters the silicate grains. The secondary calcite cement (Ccmt) lithofacies, in core description, are horizontal white beds from 1 to 2 inches. This type of calcite cement is present in the upper part of the Payne core and is characterized by surrounding the grains without significantly affecting the silicate grain compositions.

Less abundant than calcite cement, dolomite cement is present in isolated intergranular pores in the MCcSt facies. Reddish-brown Fe-Oxides are surrounding dolomite cement where dolomite is filling secondary porosity (Figure 8).

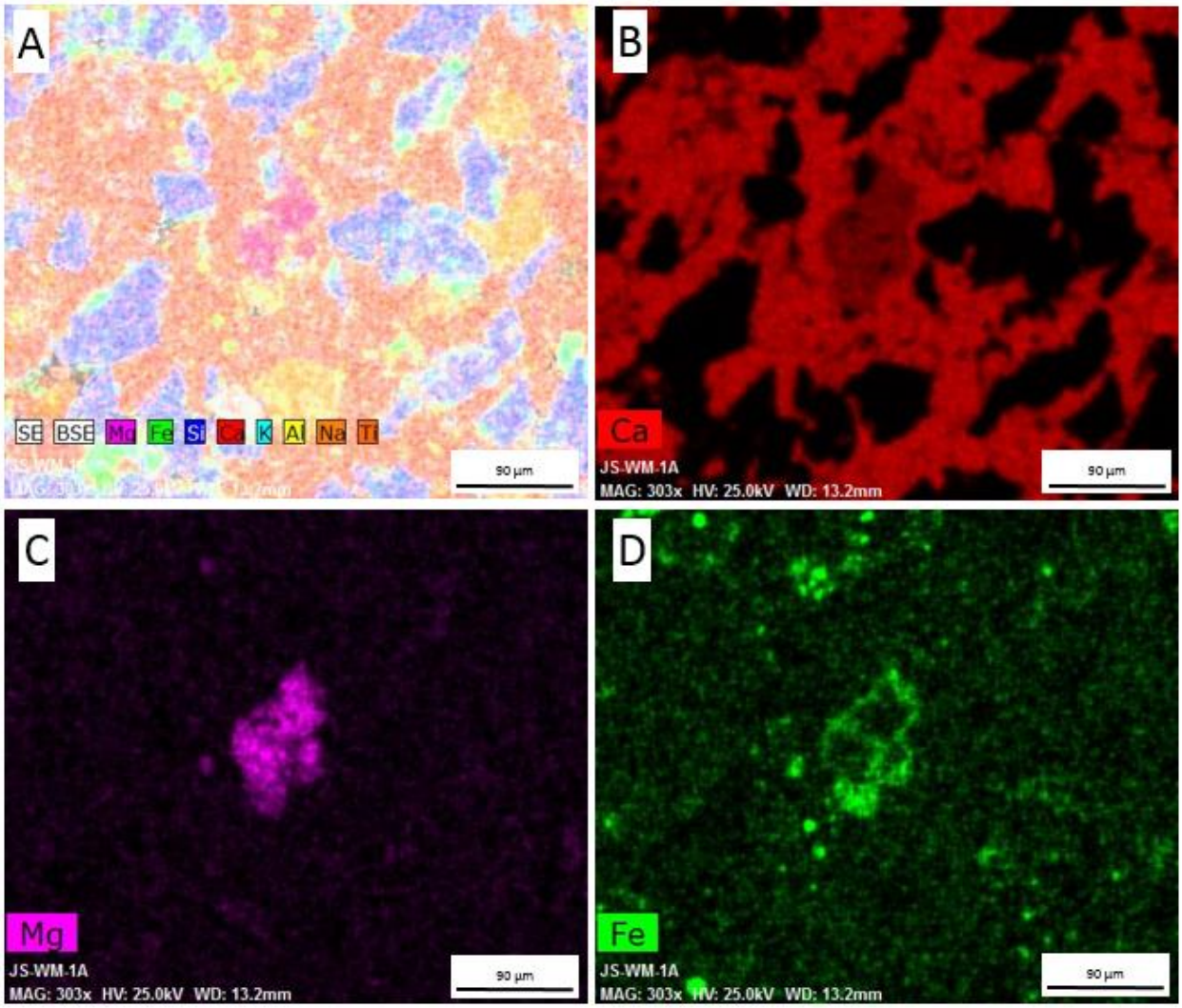

Figure 8: element maps for a sample in Payne core at 8954 ft. A) elemental map of Mg, Fe, Ca, K, Al, Na, and Ti B) calcium map. C) magnesium map D) iron map. Rhombic dolomite crystal enriched in iron at the borders.

Other types of cement were found in the systems aside from the calcite cement. Quartz cement is less abundant and fills the spaces between the crystals of blocky calcite cement in the MCcSt. Clay cement surrounds silicate grains in both calcite cement-rich and calcite cement-poor facies. Finally, diagenetic pyrite is present as framboids (Figure 9) predominantly in the bioturbated and

laminated (BSt, LSt, BMdst, LMdst) facies, but also occurs in the calcite cement-rich facies along the abundant peloids.

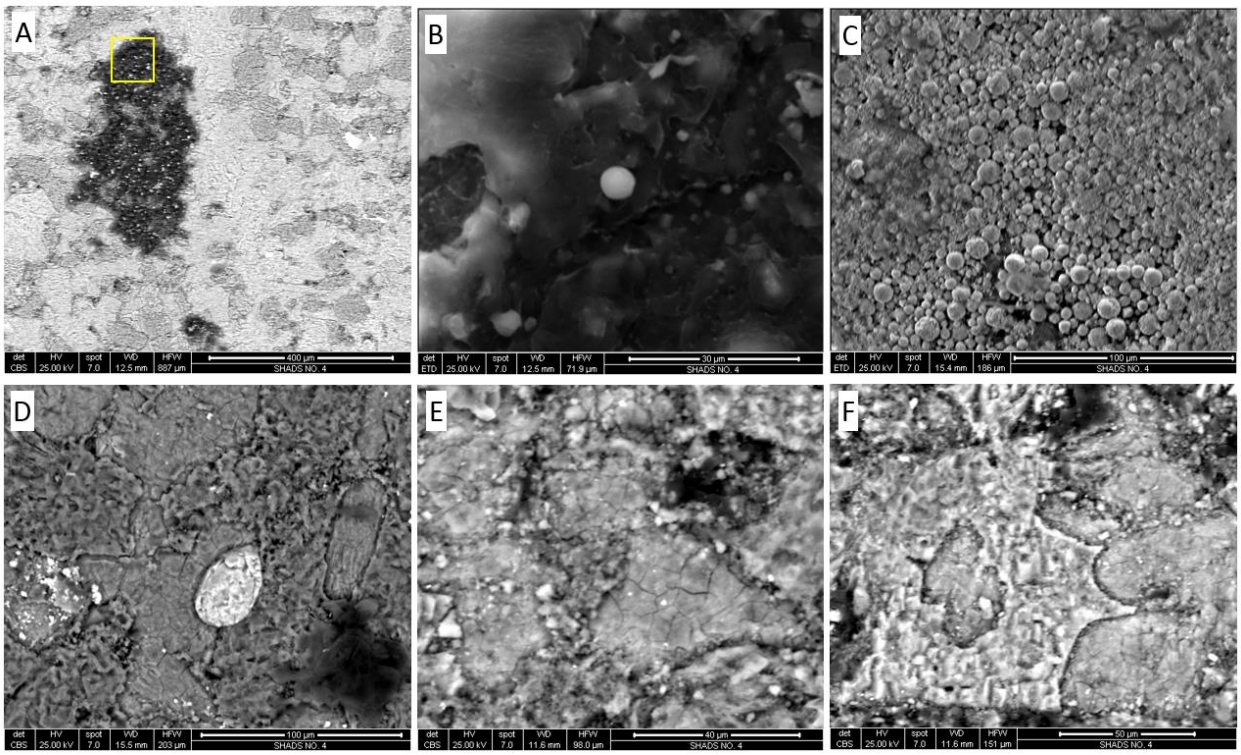

Figure 9: SEM photomicrographs. A) structural organic matter, Skaggs 9737.5 ft. B) detail of Figure 9.A. oil drop. C) pyrite framboids, Payne 8958.5 ft. D) detrital zircon, Skaggs 9741.0 ft. E) blocky calcite cement, Skaggs 9731.0 ft. F) dolomite cement surrounding calcareous grains, Skaggs 9731.0 ft.

4.2 Carbon and oxygen isotopes (δ^{13}C‰ and δ18O‰)

Isotopic values range from -5.10‰ to +1.10‰ VPDB (mean -0.92‰) for $\delta^{13}C$ and -7.60‰ to -2.20‰ VPDB (mean of -3.60‰) for $\delta^{18}O$. Three main clusters are observed in the data: facies with high calcite cement (I), facies with low calcite cement (II), and samples at the top of the section named as "Post" lithofacies (Figure 10). In the Cluster I (MCcSt lithofacies), the values of both $\delta^{13}C$ and $\delta^{18}O$ VPDB decrease with depth. For this cluster, the values of $\delta^{13}C$ range from -1.26‰ to 0.65‰ VPDB (mean -0.40‰) and the values for $\delta^{18}O$ range from -4.47‰ to -

2.37‰ VPDB (mean -3.22‰). The second cluster (II) is found in low calcite cement lithofacies. Figure 10 shows a broad range of values from -0.4‰ to +1.10‰ and from -3.22‰ to -2.20‰ of $\delta^{13}C$ and $\delta^{18}O$, respectively. The last cluster (III) is formed by samples around (above and below) to the unconformity (Post lithofacies), these samples have the most negative values of $\delta^{13}C$ vs $\delta^{18}O$.

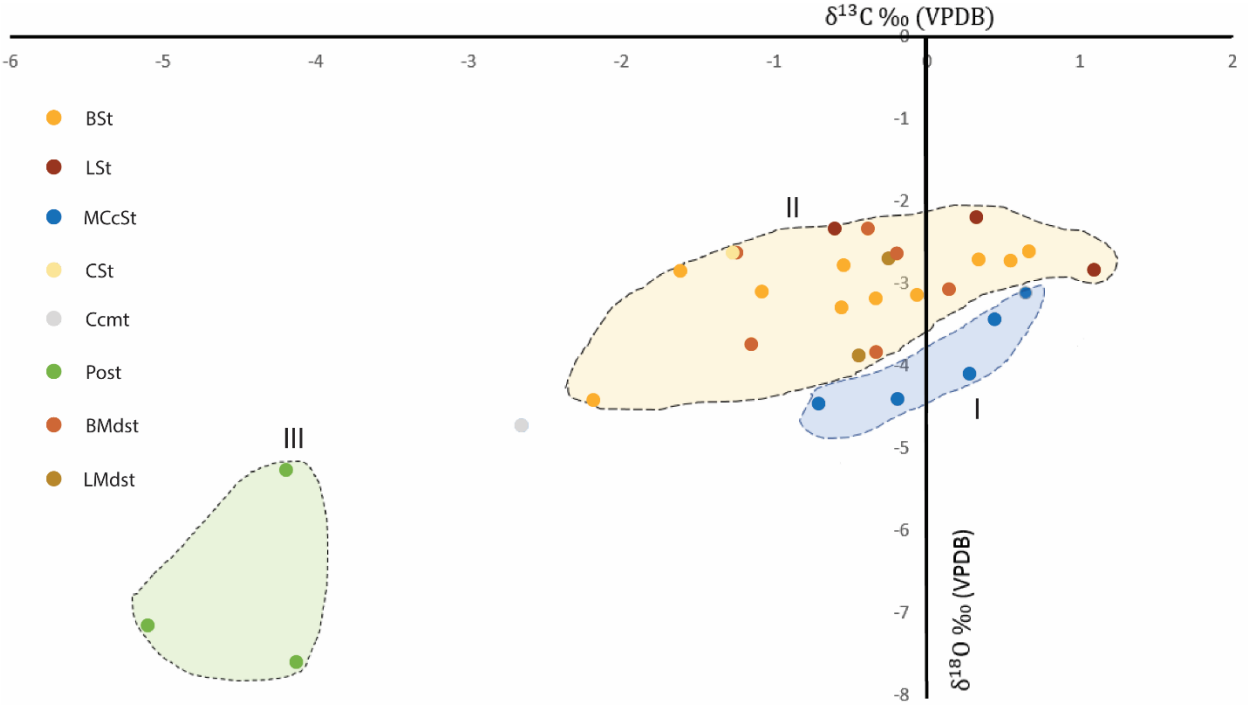

Figure 10: δ^{13} C vs δ^{18} O for Mississippian rocks in the Skaggs and Payne cores. It shows three main clusters: cluster I in blue (MCcSt), cluster II (lithofacies with low calcite content) in yellow and cluster III in green (samples were taken around the unconformity, named "Post").

To build a relative time framework, carbon isotopic composition was compared to previously built type curves (Saltzman, 2003; Batt et al., 2007; Koch et al., 2014). Skaggs core shows a jump for $\delta^{13}C$ from -4.75 ‰ to -0.45 ‰ in the contact between the Woodford and Mississippian rocks, the rest of the core range between -1.15‰ and 0.65‰ in the Payne core,

the highest $\delta^{13}C$ values is +1.10 ‰, then, the isotopic composition decreases to -5.10‰ around the Unconformity. The incursion of $\delta^{13}C$ in Chesterian time from the types curves is not present in the Merge curve.

4.3 Elemental composition variability

X-Ray fluorescence spectroscopy from a HHXRF is a semiquantitative elemental analysis technique based on the principle that each element has a characteristic combination of fluorescent (or secondary) X-Rays related to the energy lost. When an atom is excited by a primary X-Ray source the electrons are ejected, this leaves the atom unstable. Then, electrons from higher shells drop to a shell closer to the nucleus; this release of energy produces the secondary X-ray. The energy of this X-ray is used to identify each element and consequently determine the bulk elemental concentration of the sample.

The correlation matrix (Table3) shows the relationship between the elements. A positive strong relationship (K vs Al, Ca vs Sr, K vs Ti,), negative strong relation (Al vs Ca, K vs Ca, Ti vs Ca), and no significant (weak) correlation (Mg vs Al, Mg vs Si/Al, Zr vs Si/Al, Mo vs Si/Al) is given by correlation coefficients higher than 0.5, lower than -0.5, and between 0.5 and -0.5 respectively.

A positive relationship is generated because some variables are proxies interpreted from similar paleoenvironments. For example, both K and Al are proxies for clay minerals, therefore they have a positive relationship. Note that there may not always be linear trends between proxies with the same paleoenvironmental interpretation. For example, Ca and Mg are both carbonate proxies, but while calcium is associated with calcium carbonate (mainly calcite in environment conditions), Magnesium is associated with calcium magnesium carbonate (dolomite). A negative

relationship, like aluminum (clay proxy) and calcium (carbonate proxy), implies that in the system, clays and carbonates do not occur under the same conditions, in fact, one may be abundant when the other is scarce.

Direct or inverse relationship between two elements may be dependent or independent to the lithofacies. The relation between Ca and Sr (Figure 11) is an example of a relationship dependent by lithofacies. Low calcite cement facies show a linear relationship, being clear that the more calcium the more strontium. In contrast to the previous trends caused by other lithofacies, MCcSt shows an increase in Ca with the constant amount of Sr.

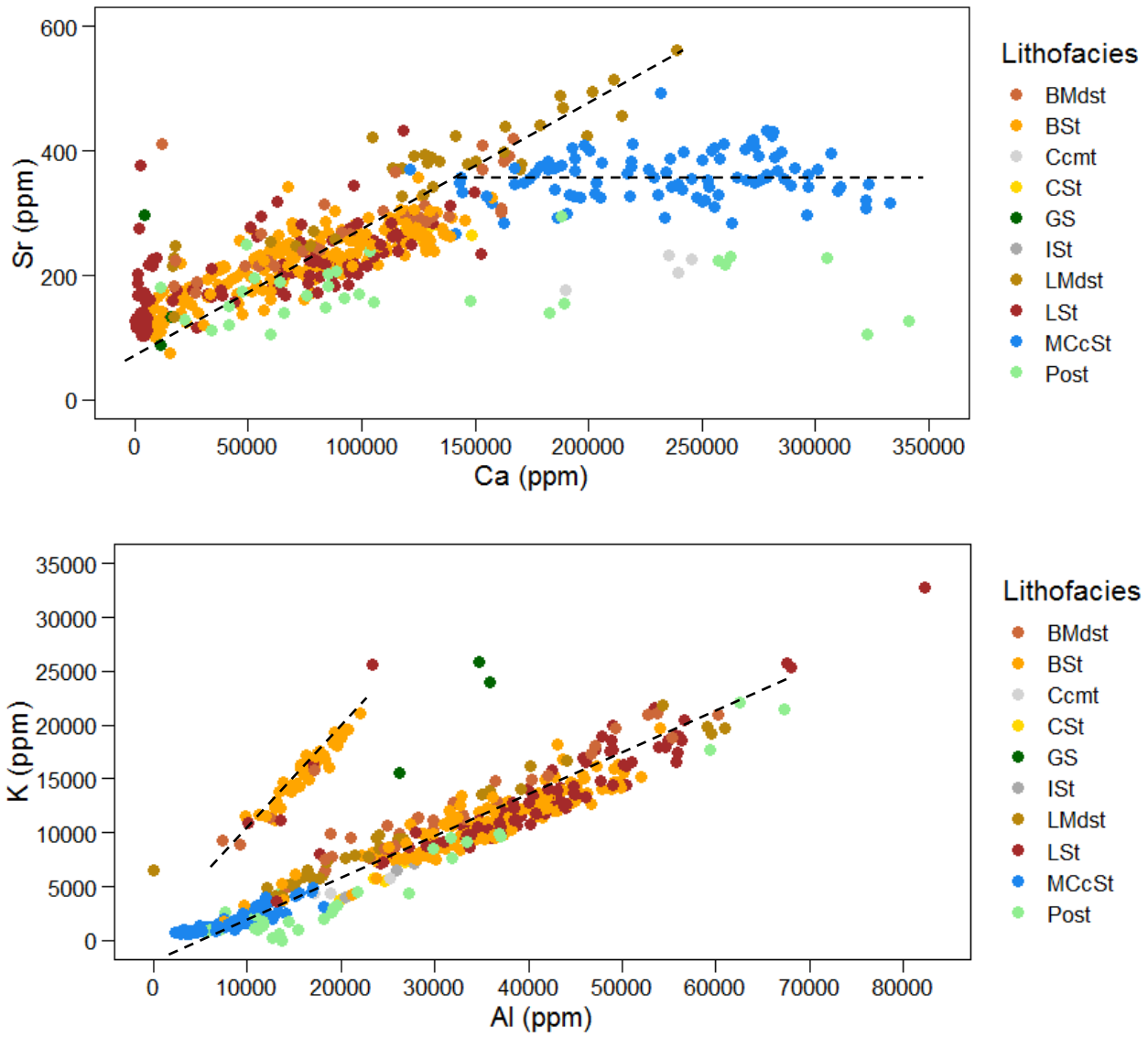

Figure 11: carbonate and clay proxies cross plots A) Relation between carbonate source proxies (Ca vs Sr). Two differentiated trends are controlled by lithofacies. While the linear direct relation is given mainly by low calcite facies, in the MCcSt lithofacies the Ca content increase with constant Sr composition. B) Relation between clay proxies (Al vs K). The cross plot differentiates two trends not controlled by lithofacies. The trend with higher slope is restricted to the lowermost section in the Payne core.

On the other hand, the cross plot between Al vs K (Figure 11) is an example of a linear relationship independent to lithofacies. In the Al vs K cross plot, two trends with the same linear positive relationship but with different slopes were identified. Most of the data lie in the lower-slope trend and only a small portion of the data lies in the trend with high slope. Contrasting to the Ca vs Sr plot, differences between the two trends in the Al vs K cross plot are confined to a specific stratigraphic section rather than dependent to different lithofacies. The high-slope trend is restricted to the lowest ten-feet section (8954 ft. to 8964 ft.) of the Payne core.

4.4 Optimal number of clusters

To define the chemofacies from the elemental composition, K-means clustering algorithm were used. For this algorithm, the number of clusters and the elements are the inputs, consequently to define the optimal number of clusters, Elbow and Silhouette methods (Rousseeuw, 1986; Thorndike, 1953) were used (Figure 12). Based on the Silhouette method two main clusters were identified, which correspond to objects with high Ca or low Ca. The Elbow method shows that after five clusters the variance does not change significantly. Thus, based on this method and after using a different number of clusters in the k-means algorithm, five clusters seem to be the optimal number of clusters (chemofacies) to find differences within low calcite cement facies. Currents studies add a PCA preprocessing step (de Lima and Marfurt, 2018; Sinha et al., 2018) to filter the data before clustering. This filtering technique will be used in the future to cluster the elemental composition data into chemofacies for Mississippian strata.

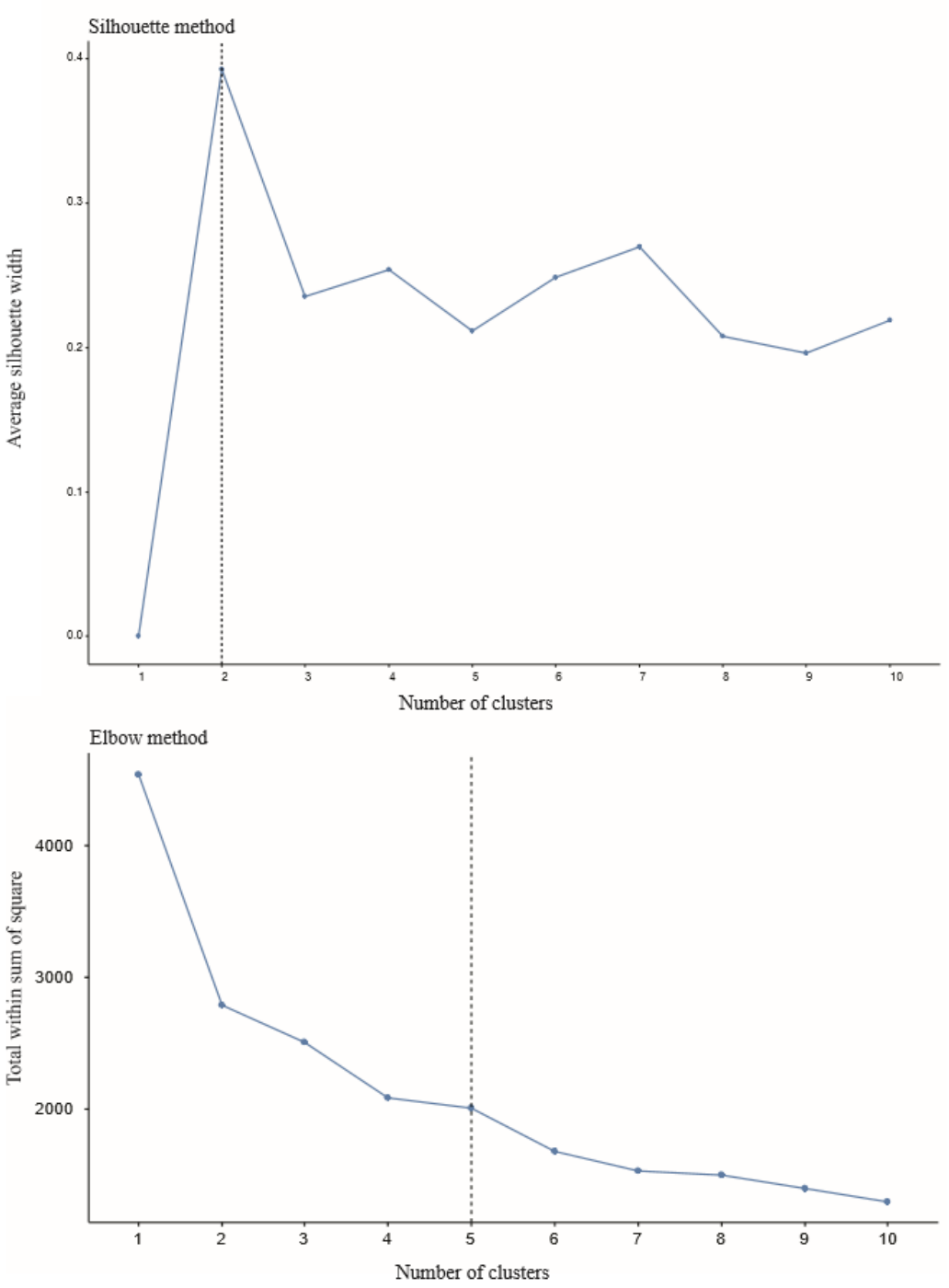

Figure 12: Silhouette and Elbow methods to select the optimal number of clusters. Silhouette (upper) and Elbow (lower) methods were used to define the number of clusters used as an input in the K-means clustering algorithm. In the Silhouette method, a high value indicates good match and a low value indicates a poor match. The Elbow method measured the distance of an object within a cluster. After 4 or 6 number of clusters, the data does not change significantly.

4.5 Chemofacies: zones with similar elemental composition

The goal to define the chemofacies was to identify differences within the two main groups of lithofacies, high calcite-cemented and poor calcite-cemented facies. Five chemofacies were defined based on the K-means (Figure 13) algorithm: dark blue, light blue, red, yellow, and green. Then, Principal component analysis (PCA) helped to define what are the most essential elements in each chemofacies.

The result of PCA are the principal components with a load of each original variable (elements) and the cumulative variance of each of the principal components (table 4). The third principal component (PC3) is chosen as the cut-off point since it accumulates a variance close to 80%, this means that the dimensions of the original data (9 variables) can be reduced to three orthogonal variables to explain about 80% of the variance within the data. The following is the importance of the original variables in the principal components: PC1 is mainly charged positively by Ca and Sr, and negatively by K, Ti and Al; PC2 is charged positively by Zr and Si/Al, and negatively by Mg; And PC3 is charged mainly by Mo. To show the importance of each proxy (original variables) in the clusters, PC1 vs PC2 were plotted using the five chemofacies from K-means as a grouping variable (Figure 13).

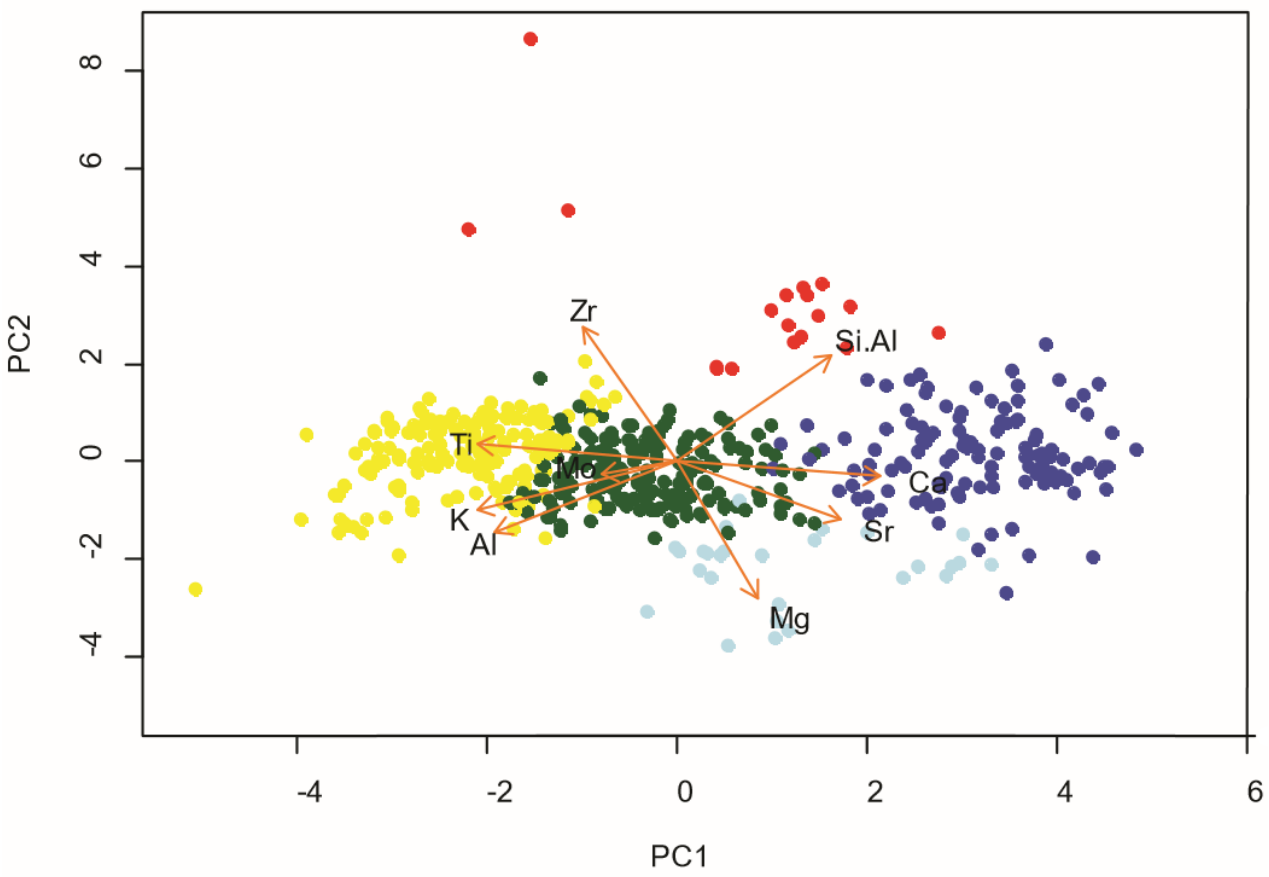

Figure 13: PC1 vs PC2 cross plot using the clusters from K-means as a grouping variable. The original variables (orange arrows) were plotted to illustrate the key elements on each chemofacies.

Because lithofacies use the mineralogical composition -thus the elemental composition- for their identification, lithofacies are linked with the chemofacies resulting from the clustering of the elemental composition (Figure 14). Accordingly, dark blue represents high Calcium and Strontium content, this chemofacies usually corresponds with MCcSt lithofacies which has high calcite content. Light blue chemofacies represents high Mg content and is common in the Skaggs core at the base of Mississippian strata. The red cluster is high in Si/Al ratio and Zr, this chemofacies is almost entirely restricted to the upper part of the Payne core (close to the unconformity) but in exceptional cases appears in the MCcSt lithofacies. Green and Yellow

chemofacies are distributed in low calcite-cemented lithofacies with similar elemental composition but differ in that yellow chemofacies has slightly more Ti, K, and Al, and the green chemofacies has more Molybdenum.

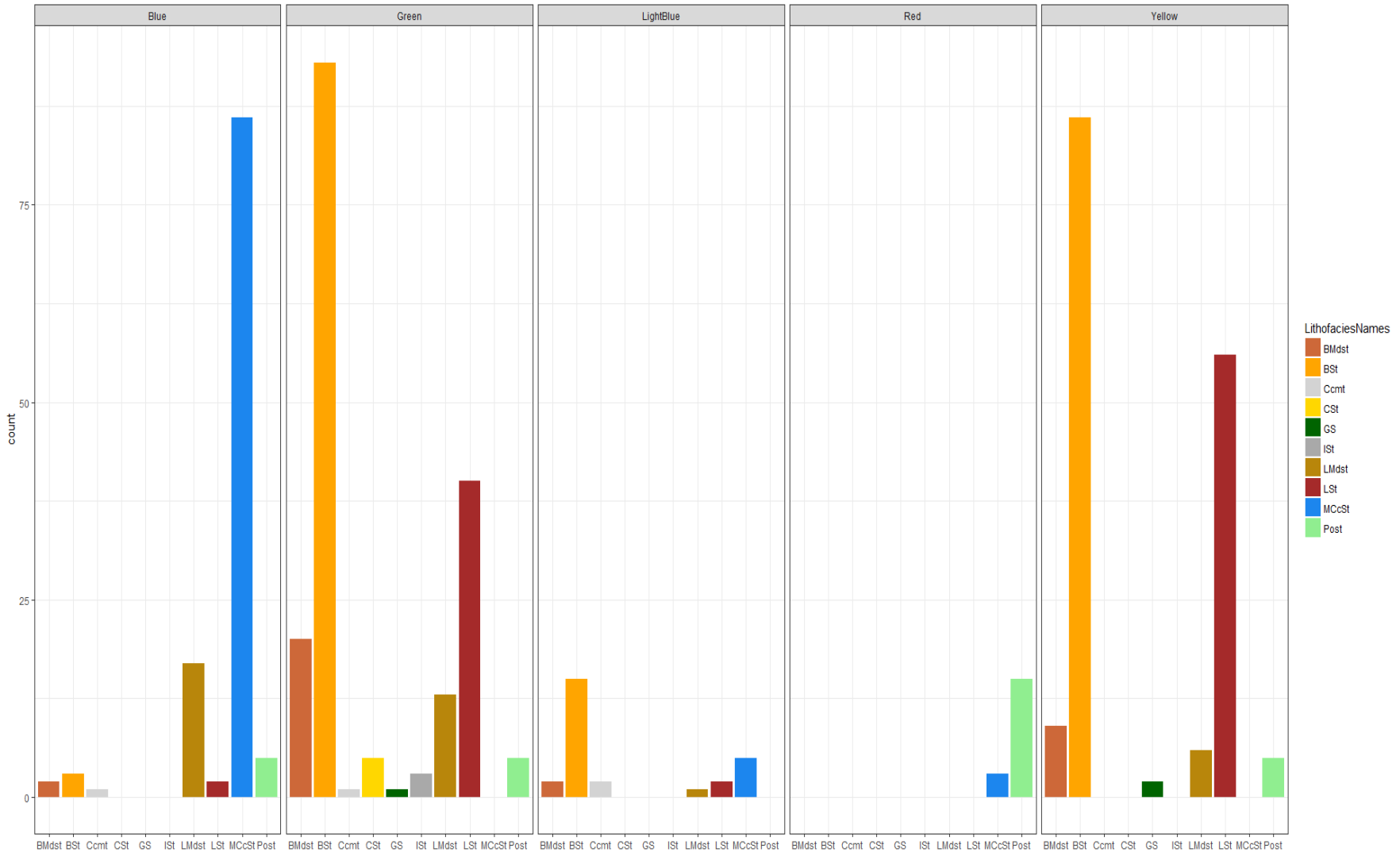

Figure 14:distribution of the lithofacies within the chemofacies. Dark blue chemofacies is related with high Calcium content; light blue with high Magnesium; red with high Si/Al and Zirconium; yellow is related with high Potassium, Titanium, and Aluminum; and green with high Mo.

4.6 Variation in elemental composition during Mississippian time

The contact between the Woodford and Mississippian strata in the Skaggs core is marked by a decrease of water bottom anoxia (Mo), and clay (Al and K) proxies, and an increase in carbonate proxies (Ca and Sr). The section between 9745 and 9750 ft. is characterized by high carbonate proxies and relative low continental proxies in comparison to the section between 9740 and 9745 ft. Despite both intervals are low calcite-cemented lithofacies, the first and deeper interval has higher amount of fossil and calcareous rock fragments. The upper section (9730-9740 ft) of the Skaggs core is marked by high carbonate proxies, low clay proxies, and high Si/Al ratio. Skaggs core has a higher amount of yellow (high in continental proxies) chemofacies at the base, and at the top it has more blue chemofacies (high in Ca and Sr).

Below 8953 ft., Payne core shows low Al but high K and Ti content. The Massive calcite-cemented siltstones in the Payne core has high carbonate proxies, but low clay and continental proxies and high Si/Al ratio. From 8943 to 8903 ft., clays proxies and Ti are increasing upward.

Strata at the unconformity and immediately below are characterized by highs and lows of carbonate, clays and continental proxies. Yellow chemofacies are more abundant at the top of the Payne core, while green chemofacies are common between 8915 and 8943 ft. Red chemofacies are mainly present in rocks surrounding the unconformity.

4.7 Sequence stratigraphy

Mississippian strata in the Merge play is bounded at the base by the Devonian Woodford shale and at the top by Pennsylvanian strata. Based on well-logs and the interpretation from the Carbon isotopes curve, it is likely that Mississippian units in the area under study correspond with a

third-order depositional sequence superimposed by smaller fourth-order sequences. Within Mississippian strata, a erosional contact at the base of MCcSt lithofacies bounds the parasequences. And within each parasequence, MCcSt are separated from bioturbated and laminated facies with transitional contacts (Figure 15). A set of these parasequences form a third-order sequence that corresponds to the gamma-ray parasequences (GRP) used to build the sequence stratigraphic framework.

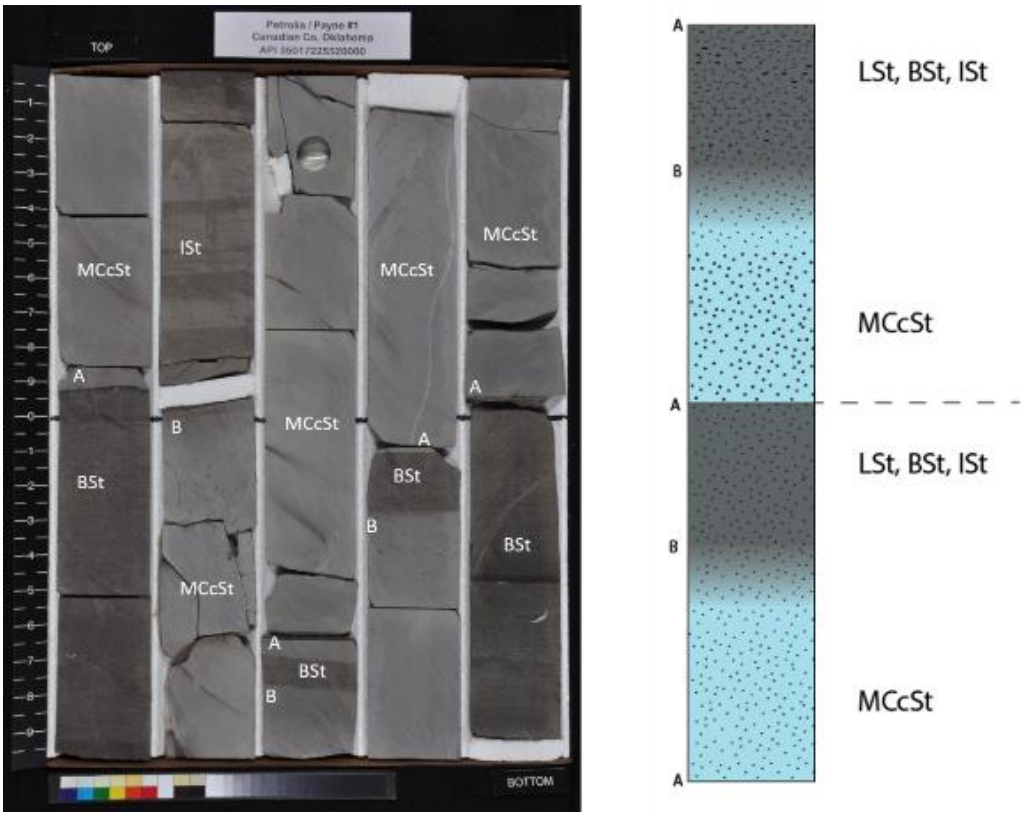

Figure 15: photo and scheme of the Mississippian strata in the Payne core. Photo of the core (left) and the scheme of the relationship between lithofacies (right). Massive calcite-cemented siltstone (MCcSt) is bounded at the base by a sharp erosional contact (A) and at the top by a transitional contact (B).

Based on the gamma-ray (GR) log response, four gamma ray parasequences (GRPs) were found (Figure 16). The first parasequence (GRP1) is bounded at the base by a sequence boundary (SB) marked by the presence of a glauconitic sandstone at the contact between the organic-rich Woodford shale and Mississippian strata. Increasing upward gamma ray represents the GRP1 and it is capped by the highest GR peak in the section. The GRP2 shows an upward decreasing GR capped by the lowest GR peak in the sections. Despite not having a core available to show the GRP2 and the lower portion of GRP3, the second sequence boundary is placed at the top of GRP2 due to a major turnaround point from decreasing upward to increasing upward GR trend. GRP3 is represented by the low GR packages thinning upward and bounded at the top by a high GR peak. Finally, a major unconformity caps the GRP4. This parasequence shows a transition from disaggregated laminated siltstones to silty micrite and sparitic siltstone rocks, immediately below the unconformity (Figure 6 & 16). The thickness of the GRP4 is variable across the area of study due to the unconformity.

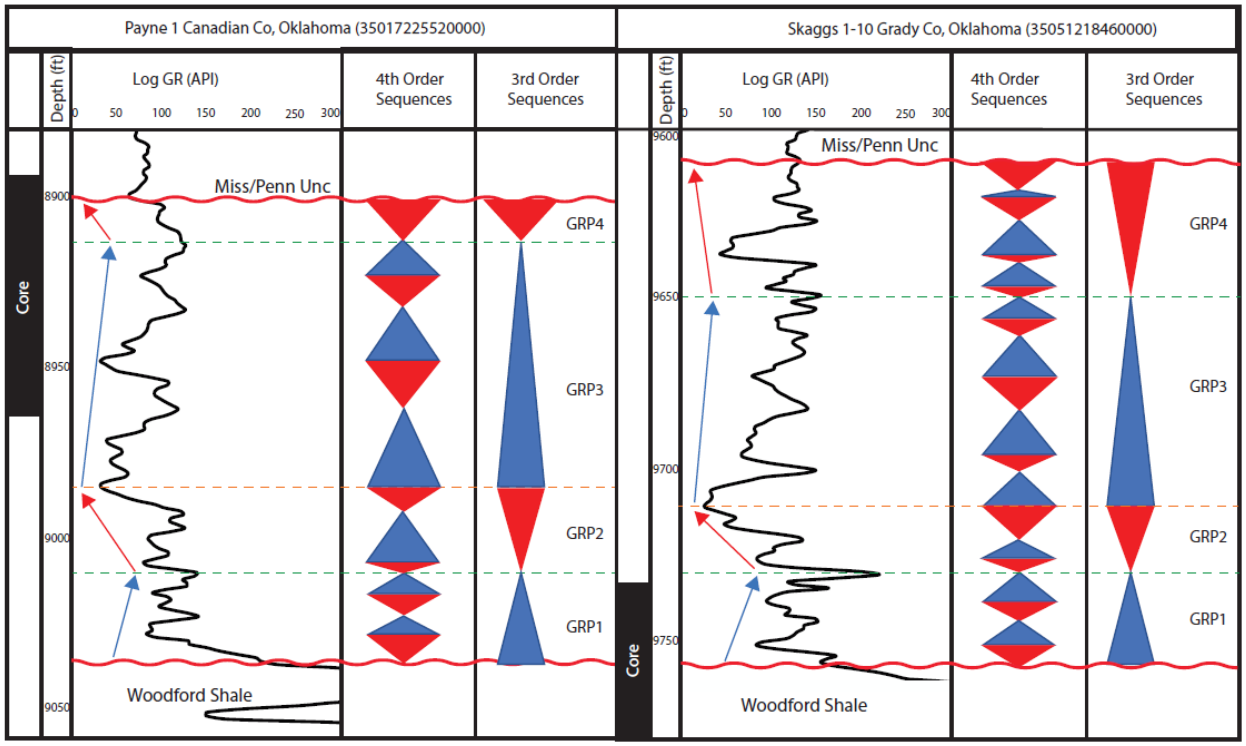

Figure 16: Gamma-ray parasequence or third-order sequences superimposed by fourth-order sequences. Black rectangles to the left represent the cored section in Payne (left) and Skaggs(right) wells. The gamma-ray parasequences are interpreted from the well-log rather than the core gamma scan.

4.8 Reservoir quality

The small number of samples may lead us to misinterpret the data. Therefore, this study avoids conclusions from lithofacies with only one sample.

Figure 14 shows the distribution of the lithofacies within the chemofacies. Blue chemofacies has a high content of MCcSt lithofacies and lower proportion of facies with low calcite cement. The green chemofacies is mainly bioturbated siltstones (BSt), but also has a high content of BMdst, LMdst. Yellow, like Green chemofacies, is absent of MCcSt lithofacies but in contrast to Green chemofacies, is also absent of Ccmt, CSt and ISt. Light blue and Red chemofacies are rear, but BSt and Post are the main lithofacies respectively within them.

Calcium is used as a proxy for carbonates, including carbonate of calcite which is controlling the reservoir quality in Mississippian strata (Price et al., 2017). Therefore, the distribution of calcium within the lithofacies (figure 17) is important to identify the lithofacies with low and high reservoir quality. The calcium in BMdst, BSt, and LSt has a broad distribution with values lower than 200.000 ppm. The MCcSt lithofacies has also a broad distribution with values higher than 100.000 ppm. The LMdst lithofacies has a distribution from values as low as 20.000 and as high as 240.000. Ccmt, CSt, GS, and ISt distribution is limited to a small range of calcium content. The Post lithofacies, located around the upper unconformity has values below 300.000 ppm for calcium content until values close to 0 ppm.

Calcium content is a key differentiator within both, lithofacies and chemofacies. Figure 18 shows the distribution of the chemofacies with respect to the calcium content. Dark and Light Blue chemofacies have high values of Ca. Contrarily, Green and Yellow chemofacies are placed in the low Ca content zone. Again, the Red chemofacies as the Post lithofacies, are distributed in most of the Ca content range due to the variability of Calcium around the unconformity.

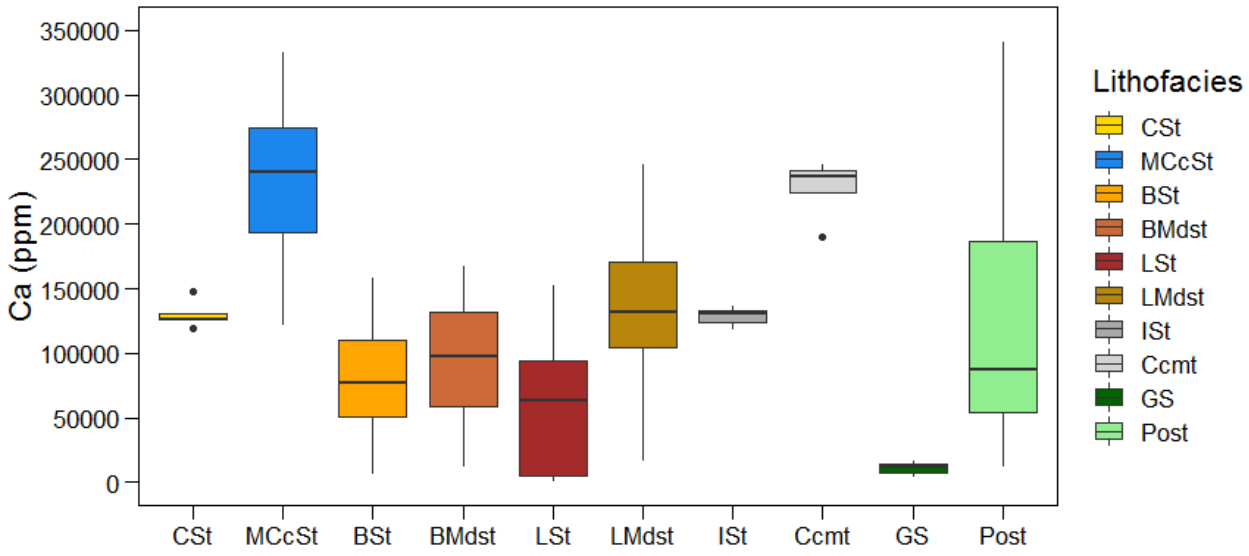

Figure 17: distribution of calcium in each lithofacies. MCcSt and Ccmt facies have the highest calcium content while the GS has the lower calcium content.

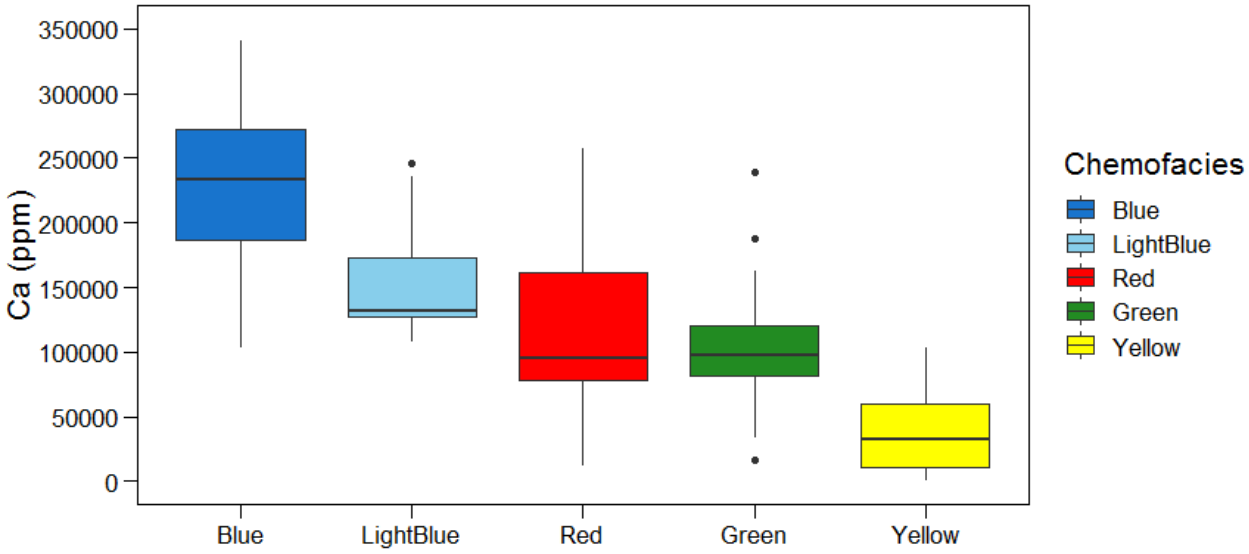

Figure 18: calcium distribution in each chemofacies. While the blue chemofacies have the highest calcium content, the yellow chemofacies has the lowest calcium content.

4.8.1 Porosity and permeability data

The distribution of porosity and permeability show most of the samples has low porosity with respect to the whole data (figure 19). Data have been divided into three intervals; most of the samples with porosity less than 4%, samples with relatively good porosity with values between 4

and 7.5%, and anomalous porosity values higher than 8%. The linear positive relation between porosity and permeability (figure 20) suggests that the higher the porosity, the higher the permeability.

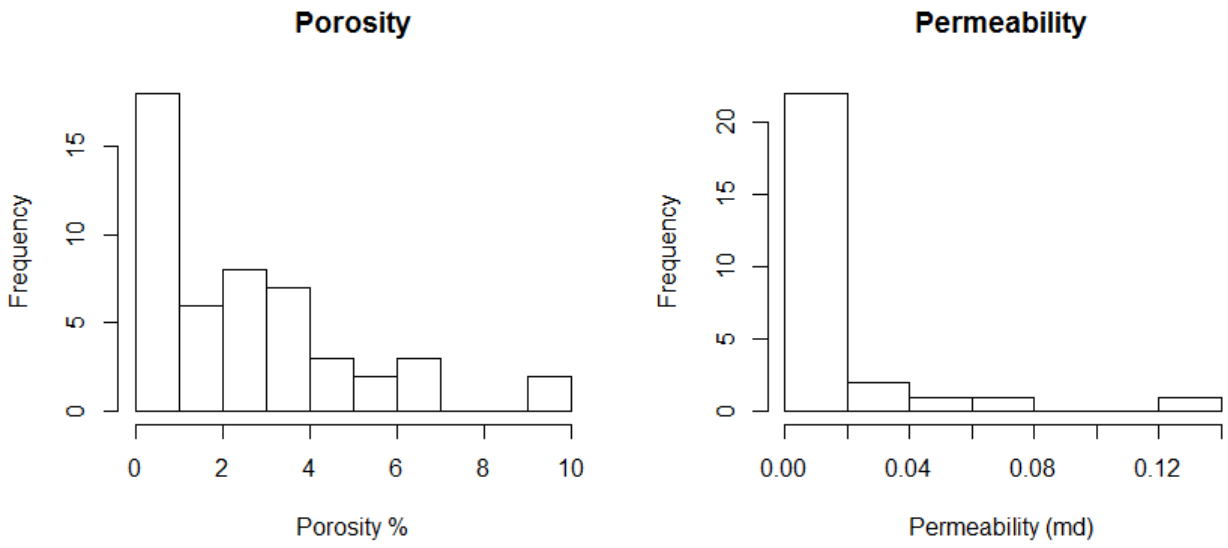

Figure 19: histogram for porosity and permeability in the Mississippian rocks.

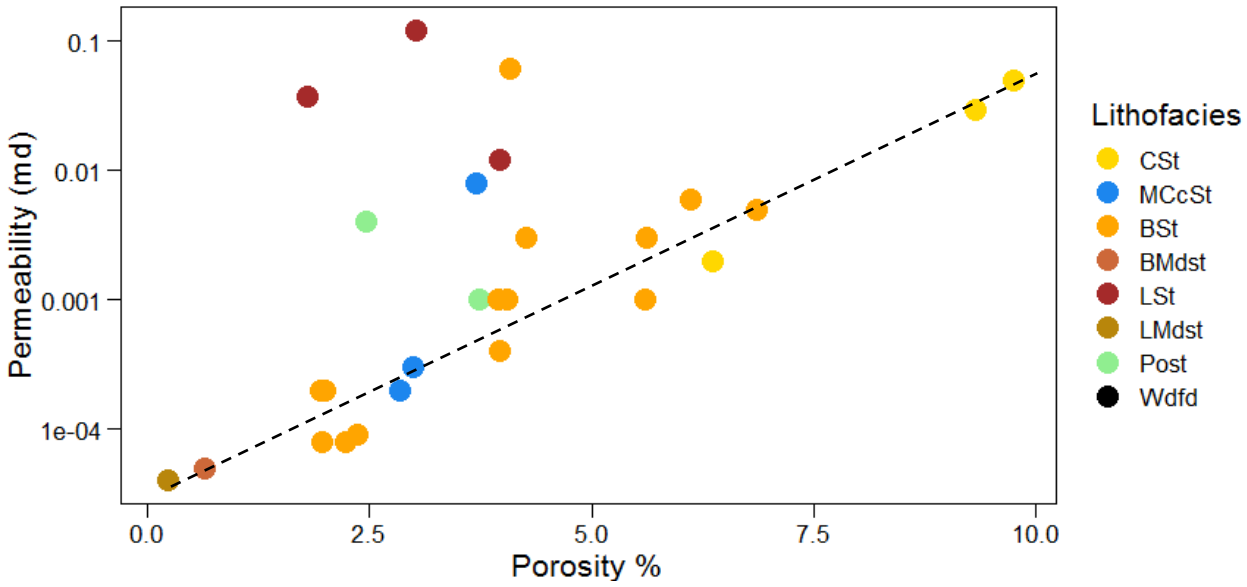

Figure 20: linear relationship between porosity and permeability in Mississippian rocks. The highest porosity and permeability values correspond to CSt facies while the lowest values correspond to LMds.

Lithofacies has different porosity and permeability values, in general. CSt is the most porous and permeable lithofaciess and BMds and LMds are the least (figure 21). But the most common lithofacies in the section are BSt, LSt, and MCcSt. Thus, within these lithofacies, BSt has higher average porosity than LSt and MCcSt. Also, LSt has higher average permeability values than BSt, and MCcSt shows the lowest permeability values within these three lithofacies (figure 22).

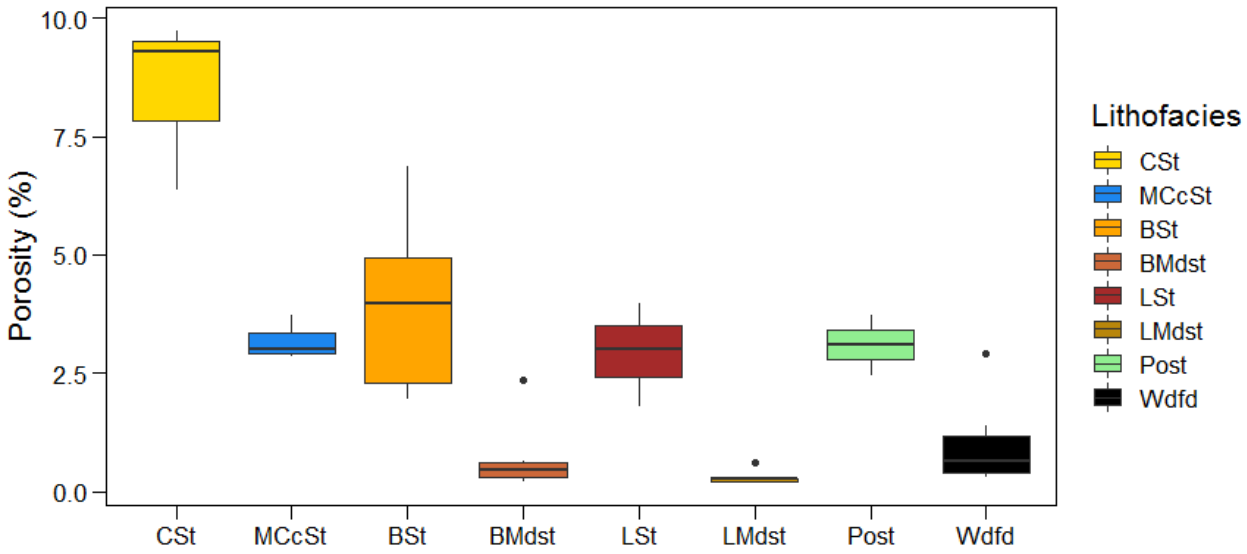

Figure 21: box plot diagram showing the porosity distribution in each lithofacies. The CSt has the highest porosity values, while the bioturbated (BMdst) and laminated (LMdst) mudstones have the lower porosity values.

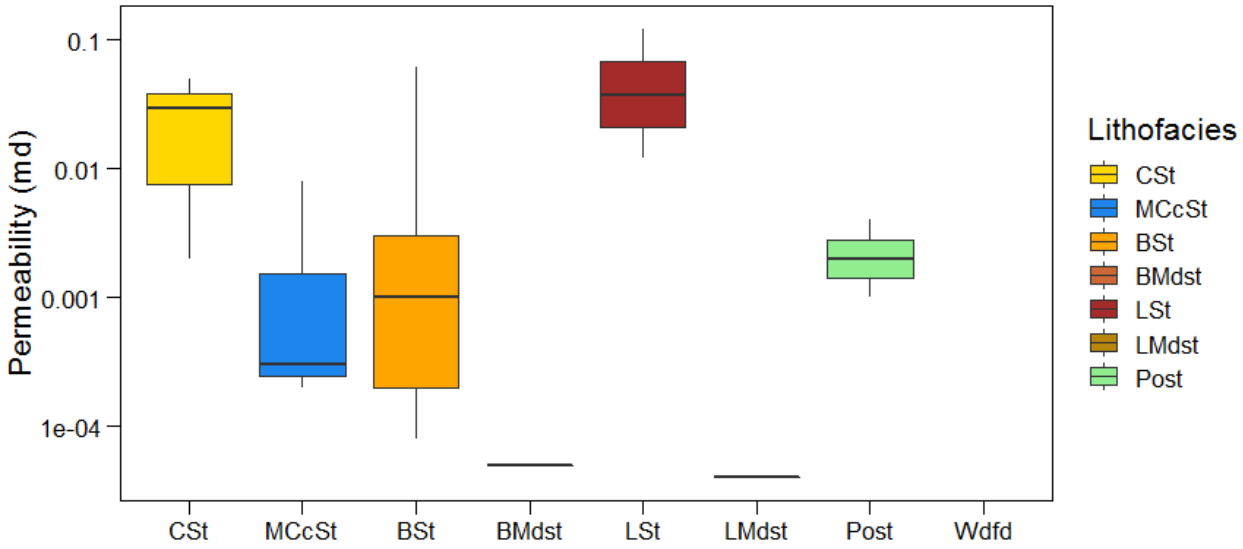

Figure 22: box plot showing the permeability distribution in each lithofacies. Only one sample was measured in each BMds and LMds.

4.8.2 Hardness

Two groups (figure 23) of rocks with hardness values dependent on the lithofacies were identified. The first group, bioturbated and laminated facies, increases the hardness of the rock with an increase of calcium content. The second group is formed mainly, but not limited to the lithofacies with high calcite cement content and is represented by a cluster of high calcium and hardness values.

The highest average hardness values in the cores (Figure 24) is the interval between 9737 and 9755 ft. in the Skaggs core. Other high average hardness values are placed in the zones with high calcium content, around 8950 ft., and around 8925 ft. The difference between these two intervals is not only the amount of calcium but also the different lithofacies with distinct types of calcite.

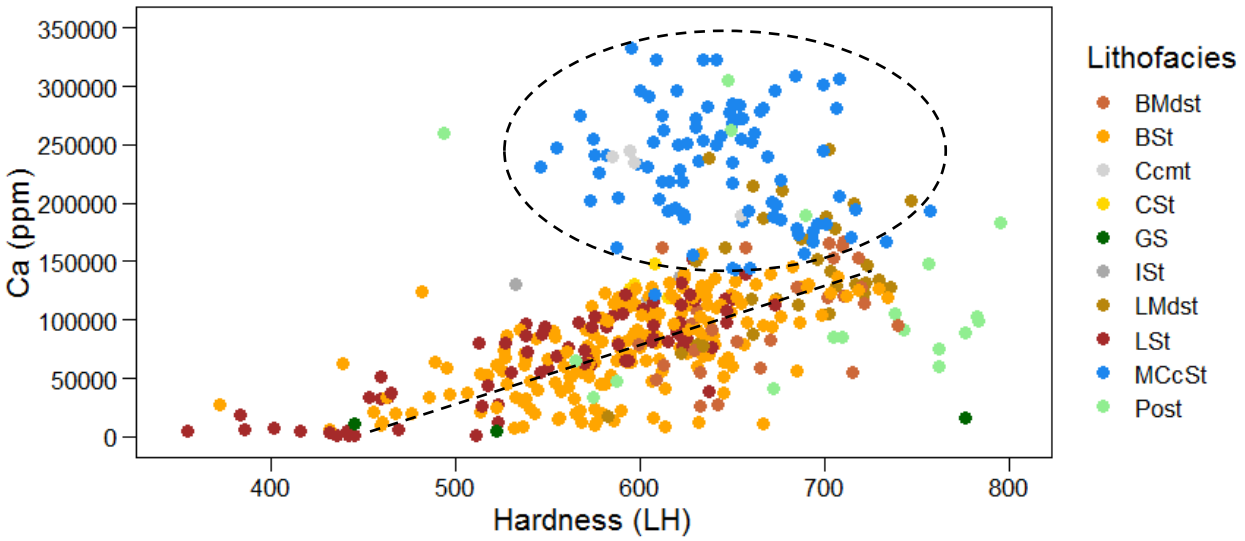

Figure 23: cross plot between hardness (LH) and calcium (ppm). Hardness values were measured with the Equotip Picolo2 hardness tester and calcium (ppm) were measured with the HHXRF.

4.8.3 Organic geochemistry

Total organic carbon (TOC) values of Mississippian rocks are considerably less than Woodford values. While TOC values for the Woodford shale in the Skaggs core go up to 5.8 wt%, within Mississippian rocks, TOC values are less than 2 wt% (table 5).

In the figure 24, the Skaggs core, which has only a portion of the GRP1, shows a decreasing upward in TOC. And the Payne core, containing the upper portion of the GRP3 and the GRP4, shows an increase of TOC until the highest value (1.96 wt%) within Mississippian rocks (top of GRP3). Then, it shows a decrease of TOC during the GRP4. In despite the upper part of the Skaggs core does not have values of S1 and S2, the S2 curve follows the same trend than the TOC in both cores. The highest TOC and S2 values are located at 9753 ft. and 9747 ft. in the Skaggs core and at 8958 ft., 8947 ft., 8930 ft. and 8918 ft. in the Payne core. S1 curve follows a similar trend than TOC and S2 curves with differences at 8947 ft., 8941ft., 8938. and 8922 ft.

The highest values of S1 are located at 9748.8 ft. and 9747 ft., in the Skaggs core and at 8958 ft., 8941 ft. and 8938 ft., in the Payne core.

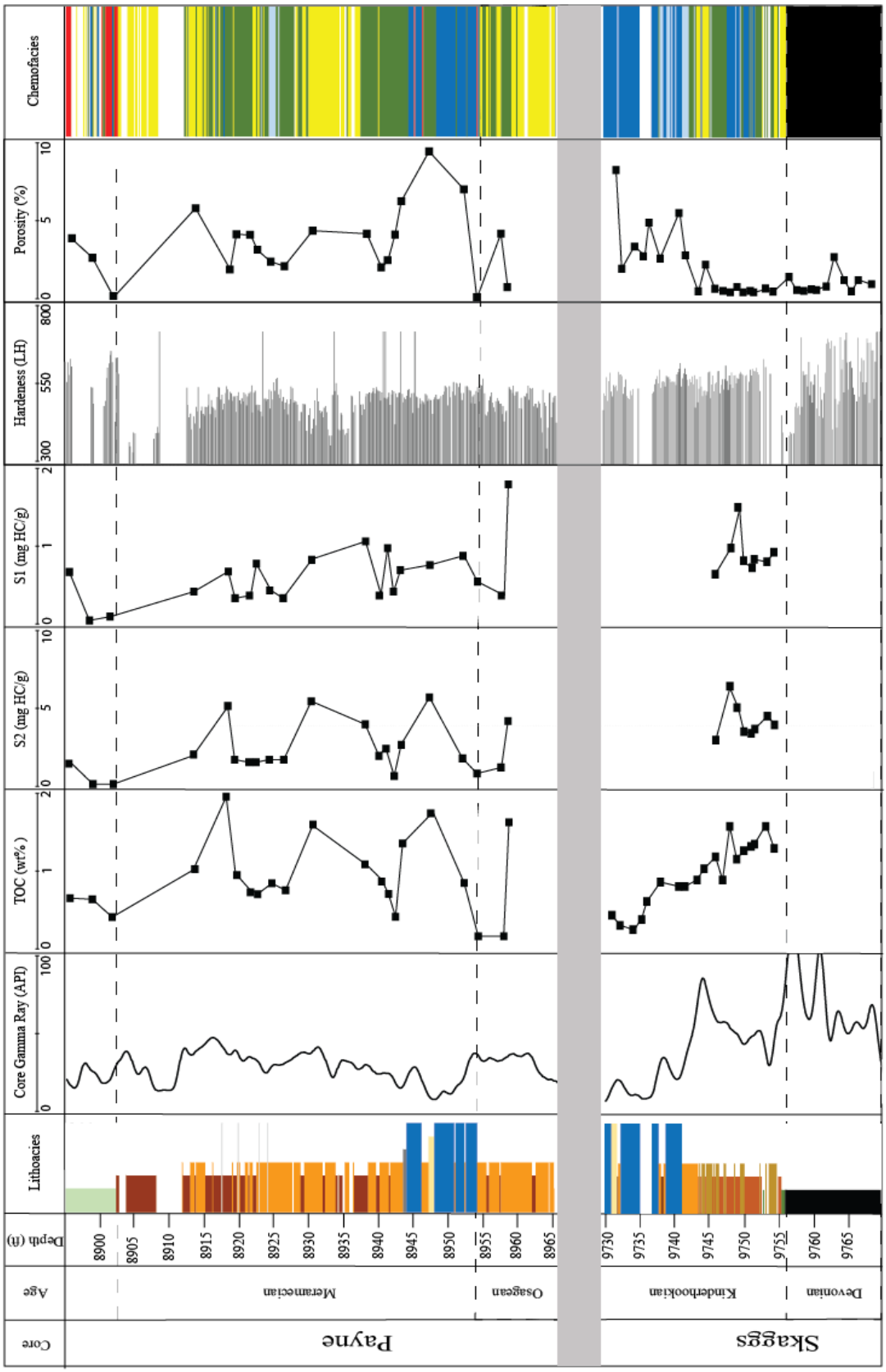

Figure 24: parameters used to evaluate the reservoir quality: lithofacies, total core gamma ray, total organic carbon (TOC), S2 peak, S1 peak, hardness data from the Equotip Picolo2 hardness tester, porosity and chemofacies.

4.8.4 Map

Based on more than 800 wells, three isopach maps from: Woodford, GRP1 and from the top of GRP1 to the Unconformity (figure 30) suggests a relationship between them. The thickest values of the Woodford are in the south-west zone of the area under study, while the thinnest intervals are in the northeast. Like the Woodford, the thinnest values of the GRP1 are located towards the northeast, in some cases, GRP1 was not present and the Woodford thins up to less than 10 ft. Excluding the northeast zone, the GRP1 thins where the Woodford thickens and vice versa. For instance, the western and southwestern part of the area shows a thick Woodford but overlying thin GRP1.

The relationship between GRP1 and the upper part of Mississippian strata (GRP2, GRP3, and GRP4) is similar to the relation between the Woodford and GRP1. The upper portion of Mississippian strata thins where GRP1 thickens. For example, while GRP1 thickens along a belt-shape from north to south, the upper portion of Mississippian strata shows the thinnest intervals.

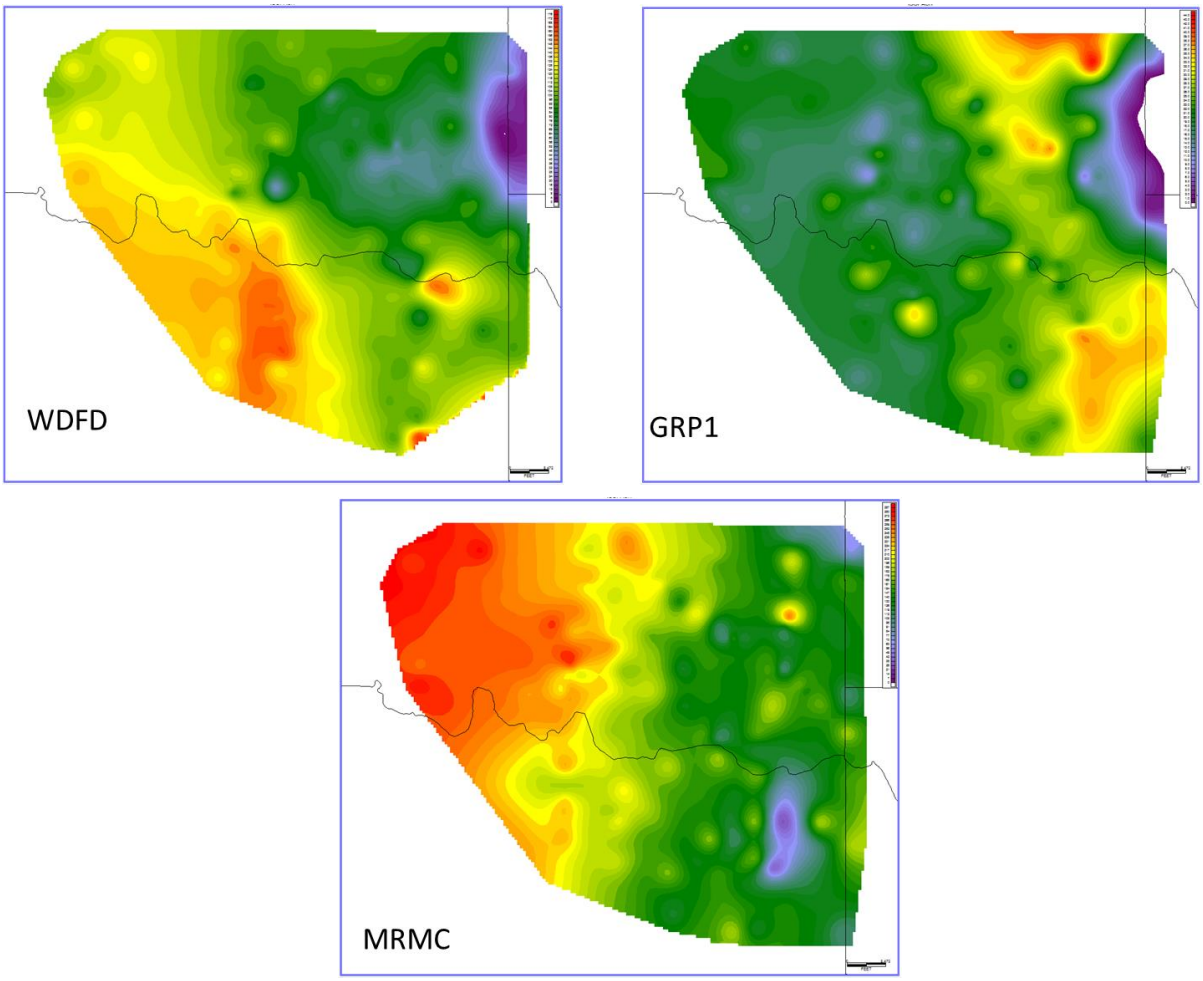

Figure 25: isopach maps from 1) Woodford, 2) GRP1 and 3) from the top of GRP1 to the Unconformity which corresponds to the Meramec (MRMC).

5. DISCUSSION

5.1. Stratigraphic description

Rather than a carbonate system (Dunham, 1962), Mississippian strata in the Merge play were deposited as a mixed carbonate-siliciclastic system and then, calcareous cement precipitated during diagenesis. The Mississippian siliciclastic strata has been interpreted as slope deposits in between shelf facies in north Oklahoma and deeper facies southeast of the area (Gutschick and Sandberg, 1983; Montgomery et al., 1998; Rogers, 2001; Loucks and Ruppel, 2007; Mazzullo et al., 2013, 2009; Koch et al., 2014;).

Unlike the STACK and SCOOP plays where the Mississippian units thicken up to 500 ft., in the Merge play Mississippian strata thins up to 120 ft. Devonian Woodford shale at and Pennsylvanian rocks bound the Mississippian strata at the top and base respectively. A glauconitic sandstone marks the lower contact, and a major unconformity, interpreted as the Mississippian / Pennsylvanian unconformity, marks the upper contact. The glauconitic sandstone at the base (Figure 3 & 5) has been reported through an extensive area of Oklahoma, suggesting a shallow marine environment. This section represents a combined sequence boundary and a transgressive surface of erosion (SB/TSE), condensing a period of time in a thin section where the lowstand system tract was not deposited. Mississippian strata thin abruptly in the Merge area due to this Miss/Penn unconformity.

Two different facies associations characterize the system: gravity flows and hemipelagic facies. Gravity flows are the massive siltstones and the hemipelagic facies are the laminated and bioturbated lithofacies. The massive calcite-cemented siltstone facies are 6 ft. to 12 ft. thick massive bodies interpreted as gravity flows. An erosional contact at the base a transitional contact at the top to finer grain facies suggest a decrease in flow regime during the

sedimentation. These contacts, the lack of the structures and the sorting in these lithofacies corroborate the hypothesis of deposition by gravity flows. Also, the well-sorted and subangular quartz grains suggest transport by suspension. The source of the sediment is still controversial; but for its geographical location (figure 1) these are the most feasible options as the source of the sediments: Transcontinental arch, Appalachian highlands, Ozark upflit and Caballos Arkansas island chain.

The abundant counterpart, bioturbated and laminated facies, are hemipelagic facies deposited on the slope between the shelf in the north and deeper facies in the south. The well-preserved peloids suggest formation in a low-energy setting related to the shelf facies in the north. Changes in sedimentation rates possibly cause differences between bioturbated and laminated facies, being higher sedimentation rates during laminated facies than during highly bioturbated facies. In the bioturbated facies, Phycosiphon, eats clay-size material and leaves behind clay-rich fecal zones (Ekdale and Lewis, 1991; Gingras et al., 2015, 2002), being important when planning a hydraulic fracture job discussed later.

5.2. Diagenesis and origin of the calcite cement

This study reveals two paragenetic sequences: 1) gravity flows facies (massive calcite-cemented peloidal siltstone and calcareous siltstones) and 2) hemipelagic facies (bioturbated and laminated facies). Calcite is present in all the lithofacies, but its amount, type and origin, differs from one facies to another. While in the bioturbated and laminated facies the allochems are the only type of calcite, in the MCcSt facies, the blocky calcite cement is the main type of calcite but there is also calcareous pellets in this lithofacies. These types of calcite have different origin and implication on the reservoir quality. Therefore, this diagenesis section gives special attention to

the blocky calcite cement lithofacies, MCcSt, due to the importance in the reservoir characterization.

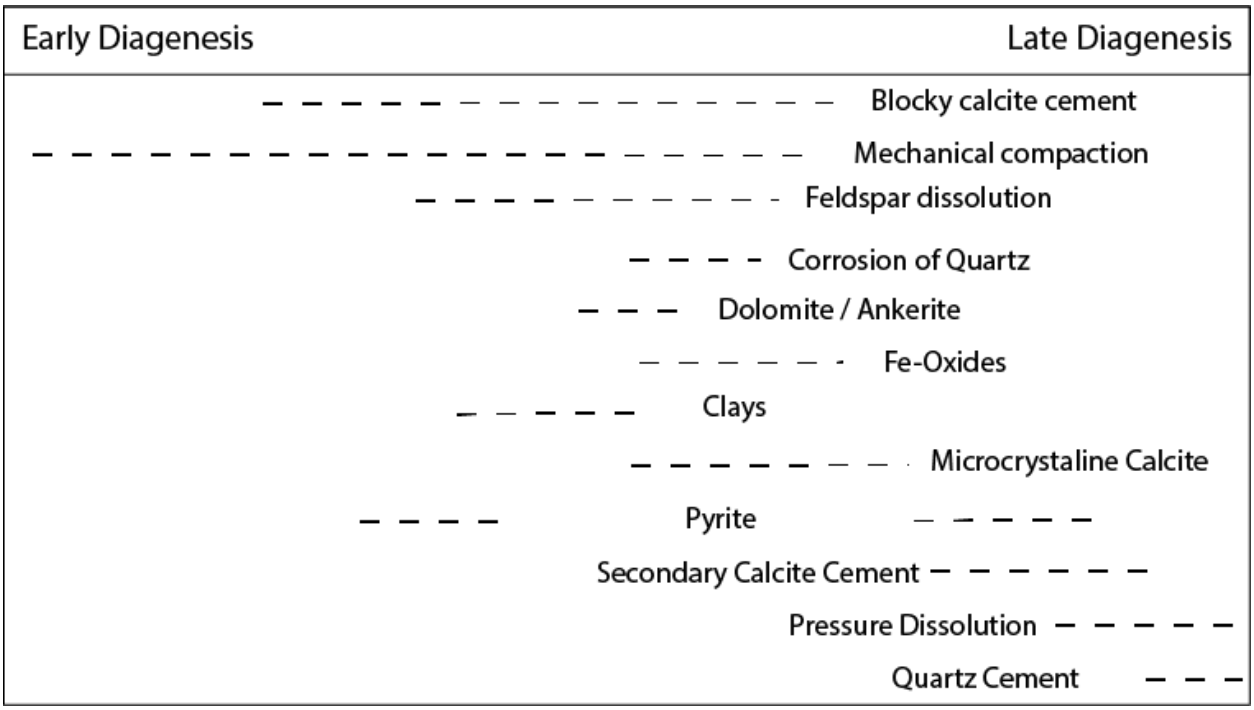

Figure 26: paragenetic sequence of Mississippian strata in the Merge area

Contrary to the general idea that blocky calcite cement precipitates on late diagenesis stages giving the floating texture (figure 26) (Moore and Wade, 2013) and based on little compaction observed and high alteration of siliciclastic grains, it seems that the blocky calcite cement within Mississippian rocks was precipitated in late early to middle diagenesis. The little evidence for mechanical compaction indicates the primary cementation occurred prior to a major burial. Additionally, in some cases, calcite cement replaces almost completely plagioclase grains and corrodes some of the more resistant quartz grains (Figure 7). This may be caused because the grains have been exposed to the calcite cement during extended periods of time. Based on the

origin of the calcite one may predict its distribution, therefore in the following paragraphs the uses of $\delta^{13}C$ and $\delta^{18}O$ are studied to interpret the origin of the calcite cement.

Carbon isotopes composition has been used to interpret the source of the carbonate that results in the precipitation of calcite. Previous studies relate positive $\delta^{13}C$ values (High amount of ^{13}C over ^{12}C) to inorganic source (Ketzer et al., 2002; Mansurbeg et al., 2012, 2009; Yuan et al., 2015; Yang et al., 2017). On the other hand, negative values of $\delta^{13}C$ results from high amount of ^{13}C related to waters enriched in CO_2 from the breakdown of organic matter (Allan and Matthews, 1977; Irwin et al., 1977; Hanor, 1978; Goldstein, 1990; Mansurbeg et al., 2012; Rahman and Worden, 2016; Li et al., 2017).

In contrast to other studies in Mississippian strata (Batt et al., 2007; Saltzman, 2003; Koch et al., 2014), most of our samples from Skaggs and Payne cores have slightly positive but mainly negative $\delta^{13}C$ values. In the Figure 10 the clusters I and II show similar trends, from more heavy isotopes (bigger values of $\delta^{13}C$ and $\delta^{18}O$) to lighter isotopes (smaller values of $\delta^{13}C$ and $\delta^{18}O$), this may indicate the same source for the carbonates in both clusters**.** While the cluster II corresponds to hemipelagic sediments, mainly calcite allochems, in cluster III the blocky calcite cement is the main type of calcite. Therefore, in the cluster I the $\delta^{13}C$ values, close to 0‰, suggest marine bioclastic source of the carbonate. Since no considerable number of fossils were observed in the massive calcite-cemented siltstones, bioclasts in the underlying and overlying hemipelagic beds are the more feasible source for the blocky calcite cement in the gravity flows (Rahman and Worden, 2016). The lowest $\delta^{13}C$ and $\delta^{18}O$ values correspond to the Cluster III, composed of samples close to the unconformity at the top of Mississippian rocks. This indicates, that unlike Cluster I and II, CO_2 resulted from the breakdown of organic matter which helped to precipitate the carbonates next to the Miss/Penn unconformity. Thus, groundwater explains

negative $\delta^{13}C$ values in rocks next to the Miss/Penn unconformity, because lighter isotopes (^{13}C) abound in biological processes that occur at the surface.

Other diagenetic minerals less relevant than the blocky calcite cement for the reservoir quality but equally important to understand the paragenetic sequence of the system are: clays, dolomite, pyrite, silica cement and late calcite cement (Ccmt). Muscovite as a detrital component has been altered, in some cases almost completely replaced by clay minerals. Thus, in the MCcSt, it is likely that alteration of smectite produced illite (Therkelsen, 2016) by interaction between acidic waters and CO_2 in contact with the micas and feldspars (Lee et al., 2010; Rahman and Worden, 2016; Wang et al., 2016).

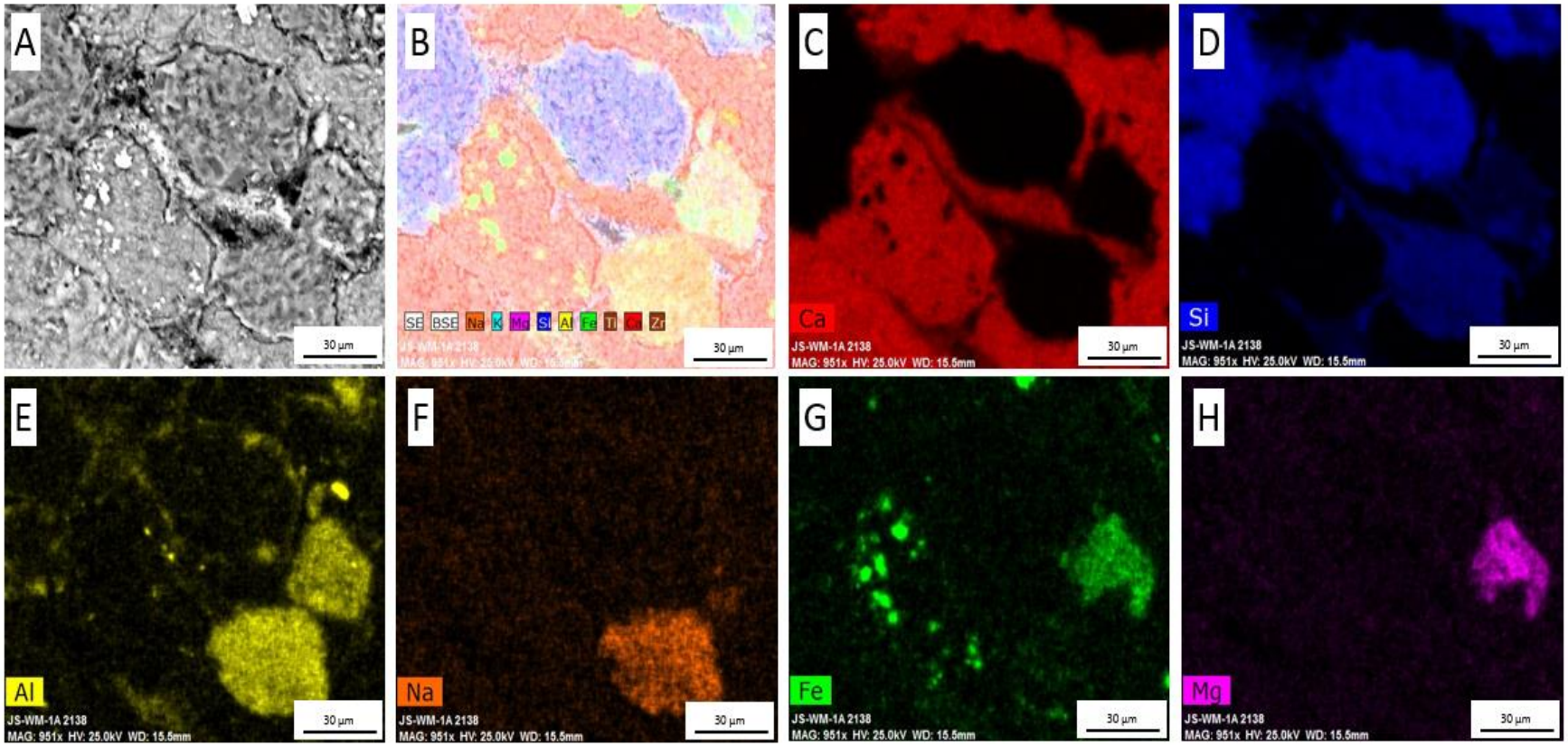

Figure 27: elements maps of sample Payne 003 at a depth of 8954 ft. A) Circular backscatter detector B) map of the elements: Na, K, Mg, Si, Al, Fe, Ti, Ca, Zr. C) calcium map D) silicon map E) aluminum map F) sodium map G) iron map H) magnesium map

Besides the calcite cement, two other cements were found: quartz cement and late calcareous cement (Ccmt). The absence of other types of quartz suggests that dissolution of detrital quartz resulted in quartz cement filling the spaces between blocky calcite cement. Calcite cement lithofacies at the top of the section, suggests that during late diagenesis, unidirectional fluids occluded the pores along two-inch zones. This calcite cement differs from the blocky cement because it is present in the bioturbated zones rather than in the MCcSt facies and does not alter the silicate grains in the same proportion as the the calcite cement. Only one sample was taken for this lithofacies, but lighter $\delta^{13}C$ and $\delta^{18}O$ values than the Clusters I and II (figure 10) suggest on organic origin for this calcite cement (Ccmt). Although this facies might not be important to reservoir quality because of its scarcity, further studies are important to understand late diagenesis in the Mississippian units.

The rhombic dolomite (figure 27) precipitated in secondary pores where dissolution from plagioclase grains occured (Figure 8). Dolomite rhombs are enriched in the center by magnesium and Fe-oxides at the borders (Figure 7).

Pyrite framboids, common in hemipelagic facies and also present in peloids of MCcSt lithofacies (figure 27), nucleated from iron monosulphides formed in oxygen-depleted environments (Wilkin and Barnes, 1997) but this system may not be deposited in a pure anoxic or euxinic environment.

This study reveals that diagenesis is not the only mechanism, but a major one driving the reservoir quality on the Mississippian mixed carbonate-siliciclastic system. Because of the low content of clays, these minerals do not affect the reservoir quality significantly. On the other hand, the blocky calcite cement, precipitated in late early to middle diagenesis occludes the

porosity in the gravity flows, therefore that study of diagenetic calcite is relevant for the reservoir quality.

5.3. Time framework

This study uses geochemistry data (isotopic and elemental composition) to build a relative time framework by correlating major changes in the composition of the rock. It is possible to build a relative time framework from $\delta^{13}C$ because the proportion of ^{13}C over ^{12}C varies over time and it is linked to the global carbon cycle (Saltzman, 2003). Additionally, major changes in elemental composition are related to changes in the source material, conditions of deposition and burial diagenesis. Therefore, by recognizing the changes of elemental composition dependent on the conditions of deposition, one may create lines equivalent in time (isochronous). For example, change in Molybdenum from the Devonian Woodford shale to Mississippian strata can be used as an isochron due to anoxic/euxinic conditions during Devonian time are more related to the Woodford than Mississippian strata.

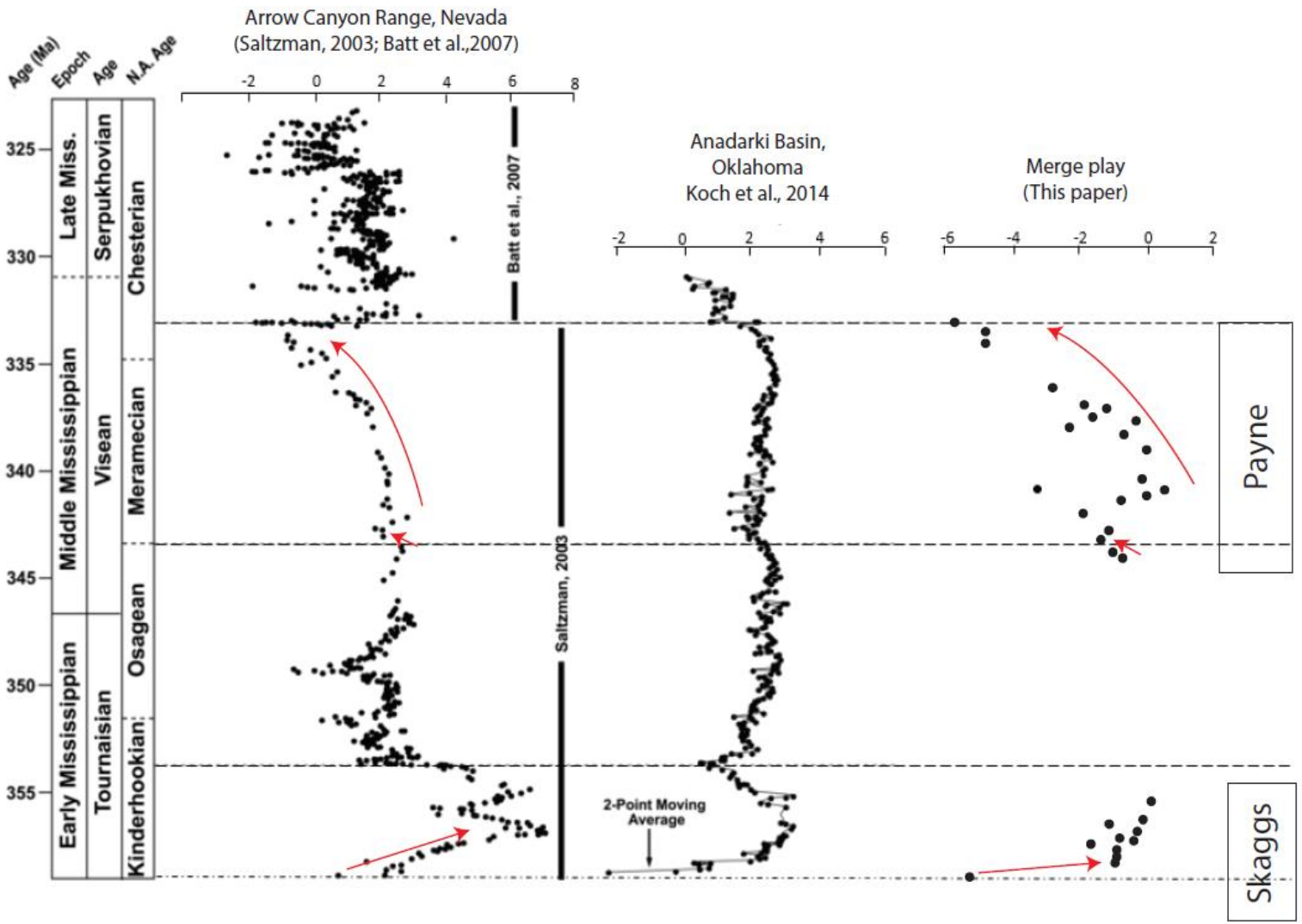

Figure 28: correlation of carbon isotopes curves in the Merge area with two type curves, one in the Arrow Canyon Range (Batt et al., 2007; Saltzman, 2003) and one in the Anadarko basin (Koch et al., 2014). Three jumps were correlated: the jump between Devonian and Kinderhookian rocks, the jump between Osagean and Meramecian rocks and the jump within Chesterian rocks (not present in the Merge area).

This study uses two type curves of $\delta^{13}C$ for time correlations: one in Arrow Canyon Range, Nevada (Batt et al., 2007; Saltzman, 2003) and one in the north part of the Anadarko basin (figure 28) (Koch et al., 2014). Based on the curve trends of the carbon isotopic composition, I identify three jumps. At the base of the section, the $\delta^{13}C$ data show an incursion from low to high $\delta^{13}C$ values also correlated with the increase in Molybdenum content. This has been interpreted as the contact between Devonian Woodford shale and Kinderhookian in age rocks.

The second jump, a slight change in the trend of $\delta^{13}C$ values, has been interpreted as the Osagean and Meramecian boundary. Elemental composition also depicts this boundary, where the interpreted Osagean in time section shows a higher slope than the remaining section in the Al vs K cross plot (figure 11B). The relationship between Al and K may be related to conditions of deposition or source material rather than diagenesis. This is important because it helps us to find changes through time. Therefore, the lower section of the Payne core corresponds to the Osagean time and the remaining section to Meramecian in time. The top of the Payne core shows a decrease of $\delta^{13}C$ without any abrupt jump. Comparing with the other curves, the Payne core does not show the jump at the base of the Chesterian age rocks. This implies that unlike the northern part of the Anadarko basin where Mississippian / Pennsylvanian unconformity is placed at the top of Chesterian rocks, in the Merge play, this unconformity eroded most of the Chesterian strata (Sutherland, 1988).

Therefore, this study provides a relative chronostratigraphic framework for Mississippian strata in the Merge play. The Skaggs core has the Devonian Woodford shale and Kinderhookian in age strata, on the other hand the Payne core has Osagean in time at the base of the core and Meramecian strata at the upper part of the core. Therefore this corroborates the hypothesis that the unconformity at the top of the section is the Mississippian/Pennsylvanian unconformity (Berg

et al., 2015; Koch et al., 2014; Grammer et al., 2013; Dolton and Finn, 1989; Bennison, 1956; Huffman and Barker, 1950).

5.4. Sequence stratigraphy

Two important sequence boundaries, the contact with the Woodford shale and the Miss/Penn unconformity bounds Mississippian strata in the merge play. This study identifies another major sequence boundary (top of the GRP2) based on the gamma ray log (figure 16). Disregarding the sequence boundaries, the Mississippian strata in the Merge area were deposited as a product of hemipelagic sediments and gravity flow events. A series of these events compose a parasequence set used to identify the gamma ray parasequences (GRPs).

Sequence stratigraphy lies on the correlation of surfaces that mark a shift in stacking patterns. Chemostratigraphy helps to correlate and interpret those stacking patterns as follows. In a siliciclastic system, a relative fall in the sea level characterizes the lowstand system tract (LST). In the LST an increase in Al-K (clay proxies) and Ti-Zr (continental proxies) depicts an increase in clastic input. Also, because LST is present in poorly oxygenated waters, one may expect high concentration levels of bottom water anoxia proxies (Mo). The transgressive system tract (TST) shows declining concentration of continental proxies (Ti and Zr) due to the relative rise of sea level. Parallel to this, the relative sea-level rise activates the bottom water circulation, this results in a declining concentration of bottom water anoxia proxies (Mo) in the column. The highstand system tract (HST) shows high concentration of clay (Al and K) and continental (Ti and K) proxies due to an increase of clastic input, but low levels of bottom water anoxia proxies (Mo) (Turner et al., 2016). Due to the absence of cored section, the use of elemental composition to

build a robust sequence stratigraphic framework was used only for the lower part of GRP1, the upper section of GRP3, and the GRP4.

The contact between the Woodford and Mississippian strata manifested by an abrupt change in elemental composition marks a sequence boundary. This sequence boundary is characterized by a decrease in bottom water anoxia concentration and an increase of carbonate proxies and bioturbation index. This is caused by the change from deeper oxic-depleted waters from the Woodford, to shallower and more oxygenated waters during early Mississippian time (Figure 3). The presence of the shallow marine glauconitic sandstone (GS) related to the transgressive surface of erosion (TSE) overlying the erosional SB (figure 5), not only implies the absence of the LST, but also the absence of significant subaerial exposure. Hence, the SB and the following transgressive period formed a single surface, sequence boundary/transgressive surface of erosion (SB/TSE), which represents a significant time lag and divides the Devonian Woodford shale from the Mississippian strata.

The GRP1 is a calcareous mudstone of Kinderhookian age, with the least porous facies within Mississippian strata and considerably less organics than the Woodford shale (table 5). Based on the lithofacies and the gamma ray response, this GRP1 is interpreted as a transition from a highly productive shale (deep environment) to less organic slope deposits. Then, not present in the cores, the highest GR peak in Mississippian strata cap the GRP1. This peak has been interpreted as a flooding surface overlying a transgressive event. This GRP1 may be correlative in time and lithology to the Kinderhook shale in the north part of the Anadarko basin (Mazzullo et al., 2009; Mazzullo, 2011) and the transition zone at the south (Milad and Slatt, 2018). Because GRP1 shows a transition from the Devonian Woodford shale to the Osagean and Meramecian age rocks, I suggest this interval should be treated as a different unconventional reservoir from the

Woodford and the younger Mississippian strata, the reason is because GRP1 has distinctive characteristics which will be discussed in the reservoir quality section.

As the upper part of the GRP1, GRP2 is not present in the cores. The decreasing upward trend from GRP2 is overlying the flooding surface from the GRP1. Despite the absence of cored strata, GRP2 is capped by a major turnaround point in the GR log. I interpreted this surface as a sequence boundary (SB2) that mark the beginning of the thinning upward sequence in the Merge play. Based on the elemental composition, it is expected that the GRP2 has a higher content of continental proxies than GRP1 but low concentration of bottom water proxies due to the circulation of bottom waters.

The GR log, lithofacies, and XRF profile shows that GRP3 is generally a transgressive event. Carbonate and continental proxies decline due to the relative increase in sea-level. Also, bottom water anoxia proxy (Mo) decreases due to the circulation of bottom waters driven by the relative increase in sea-level. At around 8,954 ft., a shift in Al, K, Ti, and Si/Al concentrations generates two slopes (Figure 11) between aluminum and potassium. The change in the slope is not dependent on the lithofacies but is restricted to a section (below 8,954 ft.) in the cores. This major change in elemental composition was interpreted as the Osagean and Meramecian boundary implying changes in conditions at the time of deposition.

The Mississippian/Pennsylvanian unconformity eroded the uppermost portion of Mississippian strata, changing the thickness of the regressive GRP4 through the area of study. This parasequence is characterized by a transition from laminated mudstone to a silty micrite and sparitic siltstone from a shallower environment. Subaerial exposure resulted in the Mississippian/Pennsylvanian unconformity and the rocks below and above the unconformity are

related to a red (high Zr and Si/Al) chemofacies (red in Figure 13) due to an increase of continental input.

5.5. Reservoir quality

Some important parameters to consider when characterizing an unconventional reservoir are organic richness, maturation, porosity and geomechanical properties (Slatt et al., 2012). Organic richness and maturation are related to the organic content in the rock; porosity is the storage capacity; and the mechanical properties, correspond to the response of the rock when applying stress. Therefore, the following paragraphs discuss the vertical variability of organic matter, porosity and hardness of Mississippian strata to identify the best landing zones.

One of the big questions is the origin of the hydrocarbons in the Mississippian strata, but this study does not pretend to define if the Mississippian units are self-source rock or a reservoir charged with hydrocarbons migrated from the Woodford. However, assuming Mississippian rocks are charged with hydrocarbons independently of the source, TOC values equal or higher than 1.5 wt% with Tmax values between 440 and 444 °C are considered mature enough to produce hydrocarbons (Law, 1999).

The S1 peak represent all the hydrocarbons in the rock, migrated and generated, hence, the three S1 peaks (9745 ft.-Skaggs, and 8655 ft.-Payne, and 8938 ft.-Payne) correspond to rock with potential to be a good reservoir. While the two lower intervals are accompanied by high TOC and S2 values, the uppermost interval corresponds to low TOC and S2 values, thus migrated hydrocarbons may charge this interval.

The second parameter, porosity, varies from one lithofacies to another controlled by the amount and type of calcite. The proportion of the lithofacies is important to evaluate the landing zone thus, the most abundant lithofacies and consequently the ones to consider when evaluating the reservoir quality are BMdst, BSt, LMdst, LSt, and MCcSt. So, the CSt which is the most porous lithofacies but the least abundant is not considered for this reservoir quality study. However, one may predict this lithofacies based on elemental composition. Intervals with high continental proxies and low clay proxies are characteristic of the gravity flows, and then carbonate proxies help to differentiate between CSt and MCcSt. Understand why the blocky calcite cement did not affect some portions of the gravity flows is the key to predict porous intervals through the Anadarko basin.

From the five most abundant lithofacies, the bioturbated siltstones and the laminated mudstones are the most and least porous respectively. The mudstones (BMdst and LMdst) in the GRP1 have similar porosity (from conventional plug analysis) values than the Woodford shale (figure 21) but less hardness values. Therefore, when planning a horizontal well, different well completion plans should be considered for the Upper Woodford shale, GRP1 (Kinderhookian in age) and the remaining Mississippian strata.

Finally, not only the amount but the type of calcite is also important in the mechanical behavior of the rock, and these differ from the gravity flows to the hemipelagic facies. While the calcite in the gravity flows is the digenetic blocky cement, in the hemipelagic flows the calcite is mainly allochems. Calcite cement in MCcSt facies produce intervals with constant high hardness values irrespective of the amount of calcite. On the other hand, in the hemipelagic facies the calcium content controls the hardness, so the more calcite the harder the rock. Therefore, the hardness in Misssissippian strata in the Merge play depends on the calcite type and amount.

Other factors when planning a horizontal well is the anisotropy of the rock. Bioturbation creates planes of weakness necessary to generate the fractures (Becerra et al., 2018). So, within the hemipelagic facies, the bioturbated intervals with high bioturbation index (Taylor and Goldring, 1993) are expected to produce fractures easier than the massive lithofacies.

Therefore, with the previous information three zones were proposed to land a horizontal well, one in the GRP1 (9745 - 9759) and two in GRP3 (8955 - 8960 and 8938 - 8941). The two GRPs analyzed have different properties when evaluating the reservoir quality. Bioturbated facies are common in these three intervals. These lithofacies have higher reservoir quality because it is not affected by the calcite cement and it is highly anisotropic due to the bioturbation. Then, hemipelagic facies with relatively high calcium content, has many plane of weaknesses to produce the fractures; are fairly hard to maintain the fractures open; and the calcite cement has not occluded the porosity.

The three proposed intervals should be analyzed based on the relationship with GRPs. These parasequences are not uniformly distributed through the area of study, instead of that, in some parts of the Merge play there is a higher proportion of GRP1 than GRP3, while in other areas GRP3 is thicker than GRP1. In other words, if targeting GRP1, the southern part of the area of study should be better because GRP1 and the underlying Woodford are thicker than other parts of the Merge play. On the other hand, GRP3 is thicker in the northwestern and thus, well targeting in GRP3 should be located in this area.

CONCLUSIONS

- Differences in geologic factors like conditions of deposition, sediment source, and burial diagenesis resulted in two major facies associations, gravity flows, and hemipelagic sediments. While gravity flows are mainly massive (unstructured) well-sorted siltstones, the hemipelagic sediments are mainly laminated and bioturbated.
- Different lithofacies were identified in the two gravity flows and hemipelagic sediments. In the gravity flows, the calcareous siltstone and the massive calcite-cemented siltstones differ in that the blocky calcite cement content is higher in latter than in the former. In hemipelagic sediments, the laminated and bioturbated facies differ in that lower sedimentation rates are expected in the bioturbated than in the laminated facies.
- Five chemofacies were identified from clustering analysis of elemental composition. 'Blue' chemofacies is related with high Calcium and Strontium; 'light blue' with high Mg; 'red' with high Si/Al and Zr; 'Green' and 'Yellow' chemofacies are distributed in low calcite-cemented lithofacies with similar elemental compositions but differ in that yellow chemofacies has slightly more Ti, K, and Al, and the green chemofacies has more Molybdenum.
- There are two main types of calcite in the facies, allochems and blocky calcite cement. Allochems (peloids, fossils, and calcareous rock fragments) were transported, most likely from the shelf in the north, and deposited in both, gravity flow facies and hemipelagic sediments. Blocky calcite cement precipitated during burial only in massive calcite-cemented siltstones of the gravity flows facies, but not in the hemipelagic facies nor the calcareous siltstones of the gravity flows.

- The amount and type of calcite control the porosity/permeability and hardness. Allochems content controls the hardness of the rock, the more allochems the harder the rock. However, this direct relationship is not conserved in the lithofacies that blocky calcite cement has precipitated (MCcSt). In the massive calcite-cemented siltstones the blocky calcite cement occludes the original porosity. Therefore, the lithofacies without blocky calcite cement have better reservoir quality.
- Petrographic analysis suggests the blocky calcite cement precipitated during late early to middle diagenesis. Stable isotopes data suggests a marine bioclastic source from surrounding beds as the origin for the carbonates in the blocky calcite cement.
- Changes in the composition of the rock, in this case isotopic ($\delta^{13}C$) and elemental composition, were used to build a relative time framework and strengthen the sequence stratigraphic model. Based on this data, it seems that the Mississippian/Pennsylvanian unconformity eroded the uppermost section of Mississippian strata in the Merge play.

REFERENCES

Algeo, T.J., Rowe, H., 2012. Paleoceanographic applications of trace-metal concentration data. Chem. Geol. 324–325, 6–18. https://doi.org/10.1016/j.chemgeo.2011.09.002

Allan, J.R., Matthews, R.K., 1977. Carbon and oxygen isotopes as diagenetic and stratigraphie tools : Surface and subsurface data , Barbados , West Indies. Geology 5, 16–20. https://doi.org/10.1130/0091-7613(1977)5<16

Allen, R.W., 2000. Complex Structural Features of the Ardmore Basin. Oklahoma City Geol. Soc. Shale Shak. 51.

Batt, L.S., Montañez, I.P., Isaacson, P., Pope, M.C., Butts, S.H., Abplanalp, J., 2007. Multi-carbonate component reconstruction of mid-carboniferous (Chesterian) seawater δ13C. Palaeogeogr. Palaeoclimatol. Palaeoecol. 256, 298–318. https://doi.org/10.1016/j.palaeo.2007.02.049

Becerra, D., Galvis, H., Slatt, R., 2018. Special section : Characterization of the Woodford Shale : Latest concepts and techniques Characterizing the two principal rock types comprising the Woodford Shale resource play : Application to shale geomechanics 6, 67–84.

Bennison, A.P., 1956. Springer and Related Rocks of Oklahoma. Tulsa Geol. Soc. Dig. 24, 111–115.

Berg, B. Vanden, Leblanc, S., Grammer, G.M., 2015. Integrated Petrophysical and High-Resolution Sequence Stratigraphic Characterization of an Unconventional Carbonate Mudrock Reservoir *, in: AAPG Annual Convention & Exhibition. Denver, Colorado.

Blakey, R., 2013. Early Mississippian paleogeography, Colorado Plateau geosystems, North America 345 Ma Mississippian (early to middle) [WWW Document].

Braun, J.C., 1961. A Stratigraphic Study of the Sycamore and Related Formations in the Southeastern Anadarko Basin. Shale Shak. Dig. III.

Burke, K., Dewey, J.F., 1973. Plume-Generated Triple Junctions: Key Indicators in Applying Plate Tectonics to Old Rocks. J. Geol. 81, 406–433. https://doi.org/10.1086/627882

Coffey, W., 2001. Lithostratigraphy and Porosity Characterization of the Sycamore Formation (Mississippian), and it's Relationship to Reservoir Performance, Carter-Knox Field, Grady and Stephens county, Oklahoma 9–17.

Culp, C.K., 1961. Stratigraphic Relations of the Sycamore Limestone (Mississippian) in Southern Oklahoma. Shale Shak. Dig. III 446–457.

Curtis, D.M., Champlin, S.C., 1959. Depositional Environments of Mississippian Limestones of Oklahoma. Tulsa Geol. Soc. Dig. 27, 90–103.

de Lima, R.P., Marfurt, K.J., 2018. Principal component analysis and K-means analysis of airborne gamma-ray spectrometry surveys, in: SEG Technical Program Expanded Abstracts 2018. Society of Exploration Geophysicists, pp. 2277–2281. https://doi.org/10.1190/segam2018-2996506.1

Dolton, G.L., Finn, T.M., 1989. Petroleum Geology of the Nemaha Uplift, Central Mid-

Continent. Denver.

Dunham, R.J., 1962. Classification of Carbonate Rocks According to Depositional Textures. Classif. Carbonate Rocks--A Symp. 108–121. https://doi.org/10.1306/M1357

Ekdale, A.A., Lewis, D.W., 1991. Trace fossils and paleoenvironmental control of ichnofacies in a late Quaternary gravel and loess fan delta complex, New Zealand. Palaeogeogr. Palaeoclimatol. Palaeoecol. 81, 253–279. https://doi.org/10.1016/0031-0182(91)90150-P

Evans, J.L., 1979. Major Structural Features of the Anadarko Basin *. Tulsa Geol. Soc. 1–13.

Feinstein, S., 1981. Subsidence and Thermal History of Southern Oklahoma Aulacogen: Implications for Petroleum Exploration. Am. Assoc. Pet. Geol. Bull. 65, 2521–2533. https://doi.org/10.1306/03B599F9-16D1-11D7-8645000102C1865D

Franklin, K.E., 1997. The depositional history of the Sycamore Limestone. Oklahoma State University.

Gingras, M.K., MacMillan, B., Balcom, B.J., Saunders, T., Pemberton, S.G., 2002. Using Magnetic Resonance Imaging and Petrographic Techniques to Understand the Textural Attributes and Porosity Distribution in {Macaronichnus-Burrowed} Sandstone. J. Sediment. Res. 72, 552–558. https://doi.org/10.1306/122901720552

Gingras, M.K., Pemberton, S.G., Smith, M., 2015. Bioturbation: reworking sediments for better or worse. Oilf. Rev. 26, 46–58.

Goldstein, R.H., 1990. Petrographic and Geochemical Evidence for Origin Of Paleospeleothems, New Mexico: Implications for the Application of Fluid Inclusions to Studies of Diagenesis 60, 282–292.

Grammer, M., Boardman, D., Puckette, J., Gregg, J., Jaiswal, P., Childress, M., Price, B., Berg, B. Vanden, Leblanc, S., 2013. Integrated Reservoir Characterization of Mississippian-Age Mid-Continent Carbonates *, in: AAPG Mid-Contienet Section Meeting. Wichita, Kansas.

Gutschick, R., Sandberg, C., 1983. Mississippian continental margins on the conterminous United States. SEPM Spec. Publ. 33, 79–96. https://doi.org/10.2110/pec.83.06.0079

Ham, W.E., 1978. Regional geology of the Arbuckle Mountains, Oklahoma. Oklahoma Geol. Surv. Spec. Publ.

Ham, W.E., Denison, R.E., Merritt, A.C., 1965. Basement rocks and structural evolution of southern Oklahoma - A Summary. Bull. Am. Assoc. Pet. Geol. 49, 927–934.

Hanor, J., 1978. Precipitation of Beachrock Cements: Mixing of Marine and Meteoric Waters vs CO2-Degassing. J. Sediment. Petrol. 48, 489–501. https://doi.org/10.1306/212F74B4-2B24-11D7-8648000102C1865D

Harlton, B., 1956. The Harrisburg Trough Stephens and Carter Counties, Oklahoma 135–143.

Hartigan, J.A., Wong, M.A., 1979. Algorithm AS 136: A K-Means Clustering Algorithm. Appl. Stat. 28, 100. https://doi.org/10.2307/2346830

Huffman, G.G., Barker, J.C., 1950. Mississippian Problems in the Lawrence Uplift , Pontotoc County , Oklahoma 22–24.

Irwin, H., Curtis, C., Coleman, M., 1977. Isotopic evidence for source of diagenetic carbonates

formed during burial of organic-rich sediments. Nature 269, 209–213. https://doi.org/10.1038/269209a0

Jones, S.C., 1988. Two-Point Determinations of Permeability and PV vs. Net Confining Stress. SPE Form. Eval. 3, 235–241. https://doi.org/10.2118/15380-PA

Keller, G.R., Lidiak, E.G., Hinze, W.J., Braile, L.W., 1983. THE ROLE OF RIFTING IN THE DEVELOPMENT OF THE Rifts are widespread in both continental and oceanic recognized as major tectonic features . The common crust and have long been association of rifts with volcanism , high heat flow , anomalous crust and mantl. Tectonophysics 94, 391–412.

Ketzer, J.M., Morad, S., Evans, R., Al-Aasm, I.S., 2002. Distribution of diagenetic alterations in fluvial, deltaic, and shallow marine sandstones within a sequence stratigraphic framework: Evidence from the Mullaghmore Formation (Carboniferous), NW Ireland. J. Sediment. Res. 72, 760–774. https://doi.org/10.1306/042202720760

Koch, J.T., Frank, T.D., Bulling, T.P., 2014. Stable-isotope chemostratigraphy as a tool to correlate complex Mississippian marine carbonate facies of the Anadarko shelf Oklahoma and Kansas. Am. Assoc. Pet. Geol. Bull. 98, 1071–1090. https://doi.org/10.1306/10031313070

Lane, H.R., De Keyser, T.L., 1980. Paleogeography of the Late Early Mississippian (Tournaisian 3) in the central and southwestern United States. Paleoz. Paleogeography West-Central United States Rocky Mt. Paleogeography Symp. 1 6, 149–162.

Law, C.A., 1999. Exploring for Oil and Gas Traps, in: Treatise of Petroleum Geology / Handbook of Petroleum Geology: Exploring for Oil and Gas Traps. American Association of Petroleum Geologists, pp. 6-1-6–41.

Lee, J.O., Kang, I.M., Cho, W.J., 2010. Smectite alteration and its influence on the barrier properties of smectite clay for a repository. Appl. Clay Sci. 47, 99–104. https://doi.org/10.1016/j.clay.2008.10.007

Leeb, D., 1979. Dynamic hardness testing of metallic materials. NDT Int. 12, 274–278. https://doi.org/10.1016/0308-9126(79)90087-7

Li, Z., Goldstein, R.H., Franseen, E.K., 2017. Meteoric calcite cementation: diagenetic response to relative fall in sea-level and effect on porosity and permeability, Las Negras area, southeastern Spain. Sediment. Geol. 348, 1–18. https://doi.org/10.1016/j.sedgeo.2016.12.002

Loucks, R.G., Ruppel, S.C., 2007. Mississippian Barnett Shale: Lithofacies and depositional setting of a deep-water shale-gas succession in the Fort Worth Basin, Texas. Am. Assoc. Pet. Geol. Bull. 91, 579–601. https://doi.org/10.1306/11020606059

Lowe, D.R., 1975. Regional controls on silica sedimentation in the Ouachita system. Bull. Geol. Soc. Am. 86, 1123–1127. https://doi.org/10.1130/0016-7606(1975)86<1123:RCOSSI>2.0.CO;2

Madden, M.E.E., 2011. X-Ray Diffraction Laboratory Manual (unpublished report). Norman.

Mansurbeg, H., Caja, M.A., Marfil, R., Morad, S., Remacha, E., Garcia, D., Martin-Crespo, T., El-Ghali, M.A.K., Nystuen, J.P., 2009. Diagenetic Evolution and Porosity Destruction of Turbiditic Hybrid Arenites and Siliciclastic Sandstones of Foreland Basins: Evidence from

the Eocene Hecho Group, Pyrenees, Spain. J. Sediment. Res. 79, 711–735. https://doi.org/10.2110/jsr.2009.060

Mansurbeg, H., De Ros, L.F., Morad, S., Ketzer, J.M., El-Ghali, M.A.K., Caja, M.A., Othman, R., 2012. Meteoric-water diagenesis in late Cretaceous canyon-fill turbidite reservoirs from the Espírito Santo Basin, eastern Brazil. Mar. Pet. Geol. 37, 7–26. https://doi.org/10.1016/j.marpetgeo.2012.03.009

Mazzullo, S.J., 2011. Mississippian Oil Reservoirs in the Southern Midcontinent : New Exploration Concepts for a Mature Reservoir Objective * 10373.

Mazzullo, S.J., Boardman, D.R., Wilhite, B.W., Godwin, C., Morris, B.T., 2013. Revisions Of Outcrop Lithostratigraphic Nomenclature In The Lower To Middle Mississippian Subsystem (Kinderhookian To Basal Meramecian Series) Along The Shelf-Edge In Southwest Missouri , Northwest Arkansas , and Northeast Oklahoma.

Mazzullo, S.J., Wilhite, B.W., Woolsey, I.W., 2009. Petroleum reservoirs within a spiculite-dominated depositional sequence: Cowley Formation (Mississippian: Lower Carboniferous), south-central Kansas. Am. Assoc. Pet. Geol. Bull. 93, 1649–1689. https://doi.org/10.1306/06220909026

Milad B. and Slatt R., 2018. Outcrop to subsurface reservoir characterization of the Mississippian Play in the SCOOP area, in: New Insights into Carboniferous Cyclothem, AAPG Midcontinent Section Fourth Biennial Field Conference. Lincoln.

Milad, B., Ghosh, S., Suliman, M., Slatt, R.M., 2018. Upscaled DFN models to understand the effects of natural fracture properties on fluid flow in the Hunton Group tight Limestone, in: Proceedings of the 6th Unconventional Resources Technology Conference. American Association of Petroleum Geologists, Tulsa, OK, USA. https://doi.org/10.15530/urtec-2018-2903038

Milad, B., Slatt, R., 2018. Impact of lithofacies variations and structural changes on natural fracture distributions. Interpretation 6, T873–T887. https://doi.org/10.1190/INT-2017-0138.1

Miller, J., 2018. Regional Stratigraphy and Organic Richness of the Mississippian Meramec and Associated Strata, Anadarko Basin, Central Oklahoma. The University of Oklahoma.

Montgomery, S.L., Mullarkey, J.C., Longman, M.W., Colleary, W.M., Rogers, J.P., 1998. Mississippian “chat” reservoirs, South Kansas: Low-resistivity pay in a complex chert reservoir. Am. Assoc. Pet. Geol. Bull. 82, 187–205. https://doi.org/10.1306/1D9BC3C7-172D-11D7-8645000102C1865D

Moore, C.H., Wade, W.J., 2013. Carbonate reservoirs : porosity and diagenesis in a sequence stratigraphic framework. Elsevier Science.

Peace, H., 1994. Mississippian Facies Relationships Eastern Anadarko Basin, Oklahoma. Shale Shak. Dig. XIII 193–202.

Perry, W.J., 1989. Tectonic Evolution of the Anadarko Basin Region, Oklahoma. United State Government Printing Office, Denver.

Pranter, M., Turnini, A., Marfurt, K., Devegowda, D., 2016. Multidisciplinary Characterization and Modeling of Mississippian Carbonate and Silica-Rich Reservoirs , Northern Oklahoma

*, in: AAPG Mid-Contienet Section Meeting. Tulsa, Oklahoma.

Price, B., Haustveit, K., Lamb, A., 2017. Influence of Stratigraphy on Barriers to Fracture Growth and Completion Optimization in the Meramec Stack Play, Anadarko Basin, Oklahoma. Proc. 5th Unconv. Resour. Technol. Conf. 1–8. https://doi.org/10.15530/urtec-2017-2697585

Price, B., Pollack, A., Lamb, A., n.d. Depositional Interpretation and Sequence Stratigraphic Control on Reservoir Quality and Distribution in the Meramec STACK Play : Anadarko Basin , Oklahoma.

Rahman, M.J.J., Worden, R.H., 2016. Diagenesis and its impact on the reservoir quality of Miocene sandstones (Surma Group) from the Bengal Basin, Bangladesh. Mar. Pet. Geol. 77, 898–915. https://doi.org/10.1016/j.marpetgeo.2016.07.027

Rogers, S.M., 2001. Deposition and diagenesis of Mississippian chat reservoirs, north-central Oklahoma. Am. Assoc. Pet. Geol. Bull. 85, 115–129.

Rousseeuw, P.J., 1986. Silhouettes: A graphical aid to the interpretation and validation of cluster analysis. J. Comput. Appl. Math. 20, 53–65. https://doi.org/10.1016/0377-0427(87)90125-7

Rowe, H., Hughes, N., Robinson, K., 2012a. The quantification and application of handheld energy-dispersive x-ray fluorescence (ED-XRF) in mudrock chemostratigraphy and geochemistry. Chem. Geol. 324–325, 122–131. https://doi.org/10.1016/j.chemgeo.2011.12.023

Rowe, H., Hughes, N., Robinson, K., 2012b. The quantification and application of handheld energy-dispersive x-ray fluorescence (ED-XRF) in mudrock chemostratigraphy and geochemistry. Chem. Geol. 324–325, 122–131. https://doi.org/10.1016/j.chemgeo.2011.12.023

Sageman, B.B., Lyons, T.., 2004. Geochemistry of Fine-grained Sediments and Sedimentary Rocks, in: Elsevier (Ed.), Sediments, Diagenesis, and Sedimentary Rocks. Amsterdam, pp. 115–158.

Saltzman, M.R., 2003. The late Paleozoic ice age; oceanic gateway or PCO (sub 2) ? Geology 151–154. https://doi.org/10.1130/0091-7613(2003)031<0151

Sinha, S., Wen, Y., De Lima, R.P., Marfurt, K., 2018. Statistical Controls on Induced Seismicity, in: Proceedings of the 6th Unconventional Resources Technology Conference. American Association of Petroleum Geologists, Tulsa, OK, USA. https://doi.org/10.15530/urtec-2018-2897507

Slatt, R.M., Mccullough, B., Molinares, C., Baruch, E., Turner, B., Column, D.S., n.d. Paleotopographic and Depositional Environment Controls on " Sweet Spot " Locations in some Unconventional Resource Shales 1 Insitute of Reservoir University of Oklahoma 3 University of Adelaide.

Slatt, R.M., Philp, P.R., O'Brien, N., Abousleiman, Y., Singh, P., Eslinger, E. V, Perez, R., Portas, R., Baruch, E.T., Marfurt, K.J., Madrid-Arroyo, S., 2012. Pore-to-regional-scale, integrated characterization workflow for unconventional gas shales. Shale Reserv. Resour. 21st century AAPG Mem. 97 127–150. https://doi.org/10.1306/13321461M97441

Sutherland, P.K., 1988. Late Mississippian and Pennsylvanian depositional history in the

Arkoma basin area, Oklahoma and Arkansas. Bull. Geol. Soc. Am. 100, 1787–1802. https://doi.org/10.1130/0016-7606(1988)100<1787:LMAPDH>2.3.CO;2

Taylor, A.M., Goldring, R., 1993. Description and analysis of bioturbation and ichnofabric. J. Geol. Soc. London. 150, 141–148. https://doi.org/10.1144/gsjgs.150.1.0141

Therkelsen, J., 2016. Diagenesis and reservoir properties of Middle Jurassic sandstones, Traill Ø, East Greenland: The influence of magmatism and faulting. Mar. Pet. Geol. 78, 196–221. https://doi.org/10.1016/j.marpetgeo.2016.09.017

Thorndike, R.L., 1953. Who belongs in the family? Psychometrika 18, 267–276. https://doi.org/10.1007/BF02289263

Tribovillard, N., Algeo, T.J., Lyons, T., Riboulleau, A., 2006. Trace metals as paleoredox and paleoproductivity proxies: An update. Chem. Geol. 232, 12–32. https://doi.org/10.1016/j.chemgeo.2006.02.012

Turner, B.W., Tréanton, J.A., Slatt, R.M., 2016. The use of chemostratigraphy to refine ambiguous sequence stratigraphic correlations in marine mudrocks. An example from the Woodford Shale, Oklahoma, USA. J. Geol. Soc. London. 173, 854–868. https://doi.org/10.1144/jgs2015-125

Wang, J., Cao, Y., Liu, K., Liu, J., Xue, X., Xu, Q., 2016. Pore fluid evolution, distribution and water-rock interactions of carbonate cements in red-bed sandstone reservoirs in the Dongying Depression, China. Mar. Pet. Geol. 72, 279–294. https://doi.org/10.1016/j.marpetgeo.2016.02.018

Wilkin, R.T., Barnes, H.L., 1997. Formation processes of framboidal pyrite. Geochim. Cosmochim. Acta 61, 323–339. https://doi.org/10.1016/S0016-7037(96)00320-1

Yang, T., Cao, Y., Friis, H., Liu, K., Wang, Y., Zhou, L., Zhang, S., Zhang, H., 2017. Genesis and distribution pattern of carbonate cements in lacustrine deep-water gravity-flow sandstone reservoirs in the third member of the Shahejie Formation in the Dongying Sag, Jiyang Depression, Eastern China. Mar. Pet. Geol. 0–1. https://doi.org/10.1016/j.marpetgeo.2017.11.020

Yuan, G., Gluyas, J., Cao, Y., Oxtoby, N.H., Jia, Z., Wang, Y., Xi, K., Li, X., 2015. Diagenesis and reservoir quality evolution of the Eocene sandstones in the northern Dongying Sag, Bohai Bay Basin, East China. Mar. Pet. Geol. 62, 77–89. https://doi.org/10.1016/j.marpetgeo.2015.01.006